Rock Mechanics and Rock Engineering (2022) 55:7243–7268
https://doi.org/10.1007/s00603-022-03010-7

ORIGINAL PAPER

Large Deformation Mechanism of Foliated Rock and NPR Anchor Cable Support Technology in the Changning Tunnel: A Case Study

Xiaoming Sun[1,2] · Bo Zhang[1,2] · Kang Yang[4] · Pengfei Guo[3] · Zhigang Tao[1,2]

Received: 22 November 2021 / Accepted: 3 July 2022 / Published online: 18 August 2022

Abstract

To solve the large deformation problem of foliated rock masses in the Changning Tunnel, rock mechanics experiments and discrete fracture numerical simulation calculations were carried out. The mechanical properties and large deformation mechanism of the foliated rock mass are analyzed. The results show a large strength dispersion in jointed rocks with different dip angles. Rock strata compression bending and shear slip caused by the rock strata structure and tectonic stress are found to be the main causes of large deformation in the Changning Tunnel. Five negative Poisson's ratio (NPR) anchor-cable support schemes were designed, and field experiments were carried out. The NPR anchor cable can maintain a constant support force to strengthen the surrounding rock and release the deformation energy by allowing the deformation of the surrounding rock through a sliding device. In the field test, the number of anchor cables in the five support schemes was gradually reduced. The reliability of these support schemes was evaluated by various monitoring methods, including surrounding rock displacement, pressure between the primary support and surrounding rock, pressure between the primary support and secondary lining, internal stress of the steel arch, and deep displacement and axial force of the NPR anchor cable. The monitoring results show that the five schemes can control the large deformation of the surrounding rock to varying degrees. The maximum deformation of the surrounding rock under the original support scheme was greater than 1 m, but the maximum deformation under the NPR anchor cable support was less than 150 mm, and the support structures were also within the safe range. Therefore, NPR anchor cable support can effectively control the large deformation of the surrounding rock in the Changning Tunnel. The research results can provide a reference for the prevention and control of large deformation in similar projects.

Highlights

- The mechanical and failure characteristics of rock samples under different joint angles have been analyzed by rock mechanics tests.
- A numerical model of the tunnel composed of triangular blocks was established, and the collapse characteristics and mechanical characteristics of the surrounding rock after excavation were analyzed.
- Five supporting schemes of "NPR long anchor cable + PR short anchor cable + W-shaped steel strip + polyester fiber mesh" were proposed and tested on site.
- The axial force of the NPR anchor cable, pressure on the primary support, pressure between the primary support and secondary lining, stress of the steel arch, deep displacement of the surrounding rock, and deformation of the initial support were monitored. The mechanical characteristics of the surrounding rock and supporting structure were analyzed, and the reasonably reserved deformation was determined. The supporting effect of the NPR anchor cable was evaluated.

✉ Bo Zhang
bqt1800605060@student.cumtb.edu.cn

1 State Key Laboratory for Geomechanics and Deep Underground Engineering, Beijing 100083, China

2 School of Mechanics and Civil Engineering, China University of Mining and Technology, Beijing 100083, China

3 School of Civil Engineering, Shaoxing University, Shaoxing 312000, China

4 Guangxi Road and Bridge Engineering Group Co., Ltd., Nanning 530200, China

Keywords Foliated rock mass · Large deformation mechanism · NPR anchor cable · Field test · Field monitoring

1 Introduction

Tunnel construction often encounters many engineering problems, such as water inrush, mud outburst, and large deformation, which endanger construction and personnel safety. For example, the continuous semiparallel excavation of the Bolu Mountain Tunnel in the process of crossing the fault caused large deformation of the surrounding rock (Brox and Hagedorn 1999). Under continuous rainfall conditions, the highly weathered andesite tuff of the Cankurtaran Tunnel in eastern Turkey softens in contact with water, resulting in damage to the support structure of the entrance section (Kaya et al. 2017). The plastic flow of the surrounding rock, the shear sliding of the wedge rock, and the bending of the thin-layered soft rock were the main reasons for the failure of the support structure in the Zhegushan Tunnel (Meng et al. 2013). Affected by the thin-layered carbonaceous slate structural effect, the surrounding rock was severely deformed after excavation, with the displacement settlement exceeding 2000 mm in the Muzhailing Tunnel (Chen et al. 2020). Under the changing in situ stress influence, large surrounding rock deformation occurred in the Sinop Dranaz Tunnel (Aydin et al. 2004). The deformation and failure factors of the surrounding rock vary, among which high geostress is an important cause, especially in the weak rock zone, which has a significant impact on tunnel construction and may lead to large deformation (Li et al. 2021; Bao 2014). In addition, the weak joints and rock composition also have a great impact on the rock mass strength, which are the reasons for the decline in rock mass strength after excavation in tunnels (Sun et al. 2017; He et al. 2013). Therefore, the problem of large deformation in soft rock tunnels is still a difficult problem in the engineering community.

The surrounding rock is in equilibrium under the influence of the geostress field before excavation. The free face appears on one side of the surrounding rock after excavation. Then, the surrounding rock will change from the original three-dimensional stress balance state to a two-dimensional stress state that easily loses stability. If enough supporting force cannot be applied to the surrounding rock, the surrounding rock may lose stability and deformation due to stress loss. The factors of large deformation include tunnel excavation, stress level, rock lithology, temperature, rock structure, fissure water, etc. Rock mass strength and geostress are the key factors affecting the stability of the surrounding rock (Hoek and Marinos 2000; Anagnostou 1993; Wang et al. 2022). Moreover, the factors affecting the rock structure, including the rock strata dip, thickness of the rock layer, and integrity of the rock mass, have a greater impact on the anisotropy of the surrounding rock (Ang et al. 2018; Yang et al. 2018; Meguid and Rowe 2006; Gao et al. 2022). In addition, large squeezing deformation of the surrounding rock is also a challenge in construction engineering (Cui et al. 2020; Liu et al. 2021; Zhang and Zhou 2017; Bosman et al. 2000; Gao et al. 2021).

At present, support measures include increasing the strength of the support structure (Chen et al. 2011), yielding support (Bonini and Barla 2012; Wu et al. 2018, 2019), flexible support (Tian et al. 2011), and prestressed bolt support (Sun et al. 2021; Zhang et al. 2022; Zhu and Ghee 2011; Tahmasebinia et al. 2018; Sengani and Zvarivadza 2018; Nguyen et al. 2015). The rock mass is the main load-bearing unit in the tunnel structure. During construction, the rock mass must be fully supported to minimize interference with the rock mass and avoid excessive damage to the rock mass strength (Aygar et al. 2020; Ng et al. 2004; Zhang et al. 2018; Zhu et al. 2021; Cao et al. 2021; Chen et al. 2022). Many experts and scholars have proposed many effective support methods for the large deformation of soft rock tunnels. Merlini et al. (2018) used shotcrete support, anchor bolt support, fiber-reinforced shotcrete, and steel arch support in solving the large deformation problem of the Ceneri Base Tunnel and effectively controlled the deformation of the surrounding rock. Dalgıç (2002) analyzed the deformation and damage caused by the strike-slip fault in the Bolu Tunnel and proposed that it could be overcome by flexible or superheavy support systems. Rahimi et al. (2014) examined the possibility of multiple block irregular failures and shallow shear failures in the surrounding rock of the Qazvin–Rasht railway tunnel and suggested the use of the "shotcrete + steel mesh + light rib steel group (IPE160)" support form. Lai et al. (2018) proposed a comprehensive support method of "advance pipe umbrella + presupport advance pipe + prestrengthening cartridge bolt + foot-locking bolt" to solve the large deformation problem of phyllite tunnels. Kimura et al. (1987) analyzed the deformation characteristics of Enasan Tunnel II, and the reason for the large deformation was the compression of the surrounding rock caused by high ground stress. Two support methods were proposed: the first is that the tunnel be excavated following the NATM excavation method, using a flexible support system to allow deformation of the surrounding rock, and the second is to resist rock pressure through a stronger support system. However, the current support technology primarily focuses on passively releasing the pressure of the support structure and improving its strength. It still belongs to the passive support method, which may not be applicable in soft rock tunnels with more complex geological conditions.

Addressing the large deformation of the foliated rock mass of the Changning Tunnel, a combined support method of "NPR long anchor cable + PR short anchor cable + W-shaped steel strip + polyester fiber mesh" was proposed. This is a high prestress compensation support method. A PR prestressed short anchor cable is used to strengthen the shallow surrounding rock to form an arch structure. The NPR high prestressed long anchor cable can not only suspend the shallow surrounding rock but also combine the deep rock mass with the shallow surrounding rock to form a double-layer reinforced arch structure to control the stability of the surrounding rock. Moreover, the constant resistance device of the NPR anchor cable can allow a certain amount of deformation of the surrounding rock while maintaining high prestress to release stress and prevent stress concentration in the surrounding rock. In this paper, the surrounding rock characteristics and initial failure characteristics of the Changning Tunnel were first analyzed. Then, the uniaxial compressive strength of standard rock samples with different joint dips was measured by rock mechanics tests to explain the influence of joint dip on the surrounding rock stability. The numerical model of a tunnel was established, and the failure characteristics, stress distribution characteristics, and plastic zone range of the surrounding rock were analyzed. Finally, field tests of five types of NPR cable anchor supports were carried out in the Changning Tunnel. The number of NPR anchor cables in each scheme was gradually reduced, and the support effect was evaluated through a variety of monitoring data.

2 Engineering Background

2.1 Geographical Position

The Chang-Bao Expressway is located in Changning County, Baoshan City, Yunnan Province. It is an important transportation line connecting Baoshan City and Changning County and plays an important role in improving local economic development (Fig. 1). At present, the construction of the Chang-Bao Expressway has been completed except for the Changning Tunnel. The construction progress of the Changning Tunnel was very slow due to a series of geological disasters such as large deformation of asymmetric soft rock, water inrush, mud inrush, and collapse.

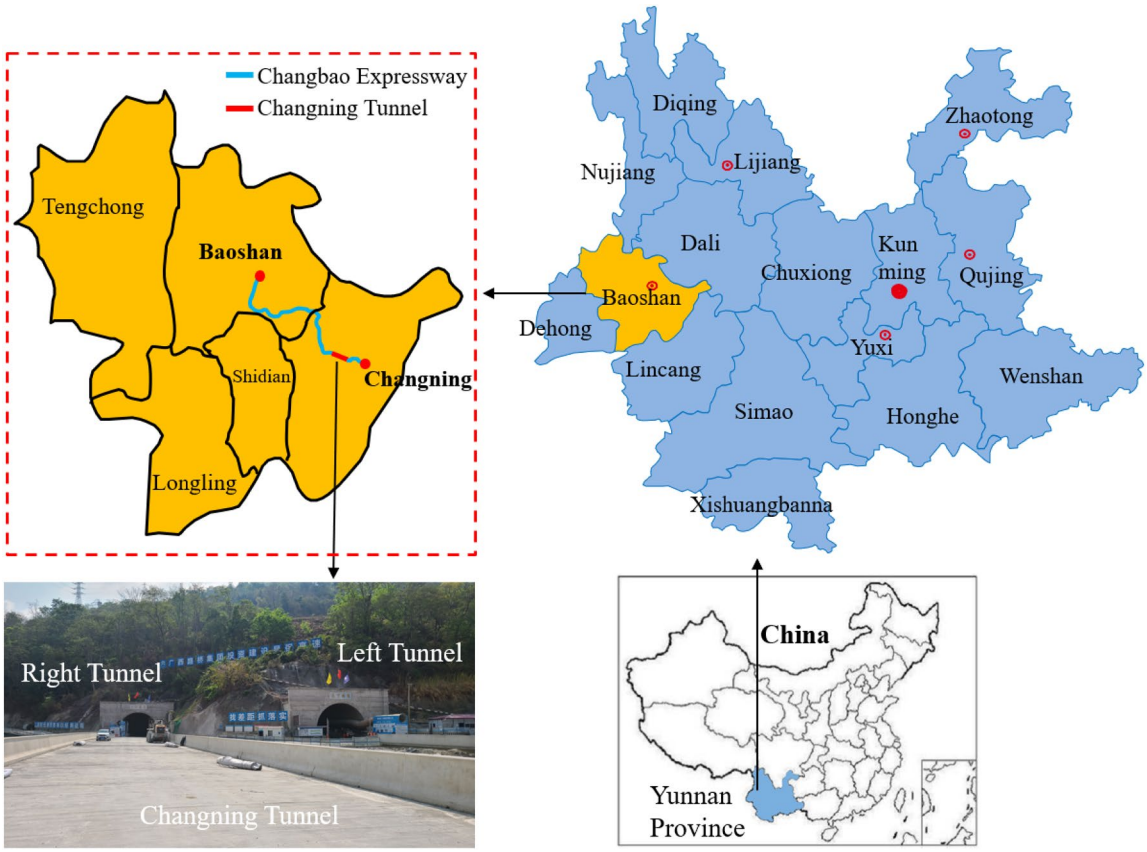

Fig. 1 Location of Changning Tunnel

2.2 Geological Conditions

The Changning Tunnel is a separate two-hole four-lane expressway tunnel with a design speed of 80 km/h. The starting mileage of the right tunnel is YK28 + 031, and the ending mileage is YK33 + 456, with a total length of 5,425 m and a maximum buried depth of approximately 416 m. The starting mileage of the left tunnel is ZK28 + 058, and the ending mileage is ZK33 + 510, with a total length of 5,452 m and a maximum buried depth of approximately 456 m. The elevation of the tunnel area is between 1470.0 m and 2038.0 m, and the relative elevation difference is approximately 568 m. It is in a mountain area with denudation and topographic fluctuation. The section with a burial depth of more than 300 m accounts for 40.5% of the total length. The excavation span of the two tunnels is 12 m, the height is 10 m, and the distance between the two tunnels is 20 m.

As shown in Fig. 2, the fault is developed, and the main faults that the tunnel passes through are F30, F32, and F33. Fault F30 (47°∠60°) is an inactive strike-slip fault with a width of approximately 80 m. Fault F32 (73°∠65°) is an inactive strike-slip fault with a width of approximately 100 m. Fault F32 (73°∠65°) is an inactive strike-slip fault with a width of approximately 80 m. The faults consist of crushed rock and argillaceous filler, with low strength and easily collapsed after excavation (Fig. 3). As shown in Fig. 4, the rock stratum is complex, and the surrounding rocks are moderately weathered metamorphic sandstone intercalated with schist. In addition, it also includes dacite, sandstone, sandstone mixed with conglomerate, limestone mixed with metasandstone, etc. The test tunnel section is buried between 360 and 390 m. The exposed surrounding rock on the face of the tunnel is shown in Fig. 5. The structural forms of the surrounding rock include fault development, orderly structural rock stratum, and disordered structural rock stratum. The joints and fissures are developed in layered and foliated structures. The dip angle of the rock stratum is between 7° and 15°, and the thickness is between 10 and 60 mm, which is not uniform. The mineral components of rock are quartz and clay minerals. Clay minerals include illite and chlorite, accounting for approximately 48%. In its natural state, chlorite schist tends to soften and decompose when it contacts water. According to the geological survey data, the average compressive strength of the rock mass is 10–60 MPa, the tensile strength is 2.1–3.6 MPa, the Poisson's ratio, cohesion, and internal friction angle are 0.19–0.22, 0.5–0.6 MPa, and 22°–28°, respectively. The maximum principal stress is horizontal in the tunnel site, reaching 15–18 MPa, with a dominant direction between NW38 and NW51°. The vertical stress is approximately 8.5. Due to the broken rock mass, the development of fault structure, and fissure water, there are great hidden dangers of water inrush, mud inrush, and collapse.

2.3 The Original Support Design of the Tunnel

As shown in Fig. 6a, the excavation method was a three-bench seven-step excavation method with reserved core soil (TSEM) (Li et al. 2016). The lengths of the three benches (upper, middle, and lower) were 3–5 m, 3–5 m, and 8–10 m,

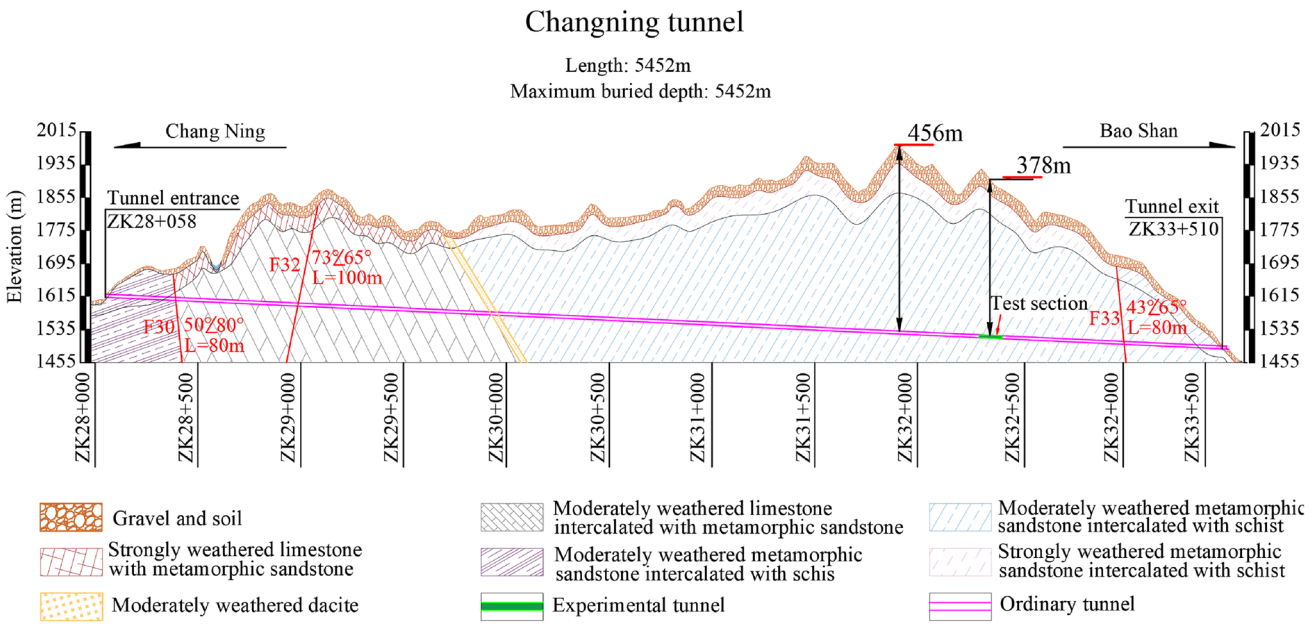

Fig. 2 Longitudinal geology profile and test section of the Changning Tunnel

Fig. 3 Surrounding rock collapse at fault

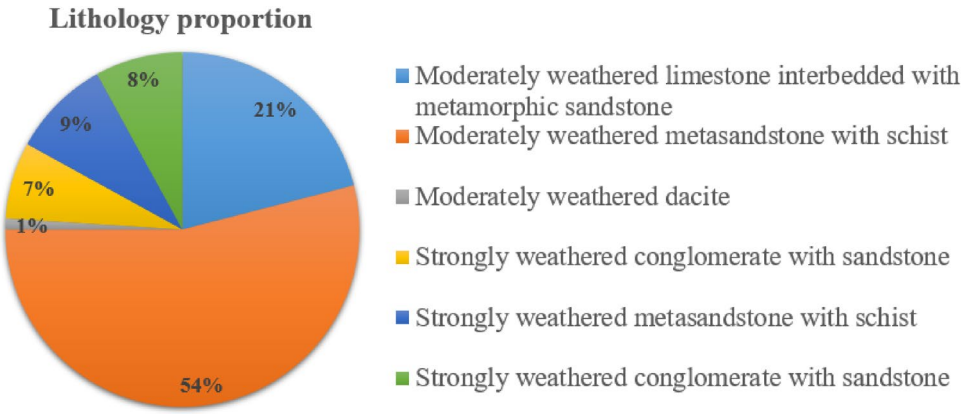

Fig. 4 Proportion of different rocks in the tunnel

(a) Fault development (b) Orderly rock stratum (c) Disordered rock stratum

Fig. 5 Surrounding rock of the tunnel face

respectively. The original support design was a composite support form (Fig. 6b), and the I22a type steel arch and hollow grouting bolts (3.5 m) were used to support the excavated rock mass. As shown in Fig. 6c, since the implementation of the scheme, the average daily deformation of the primary support structure was 1–2 cm, the deformation

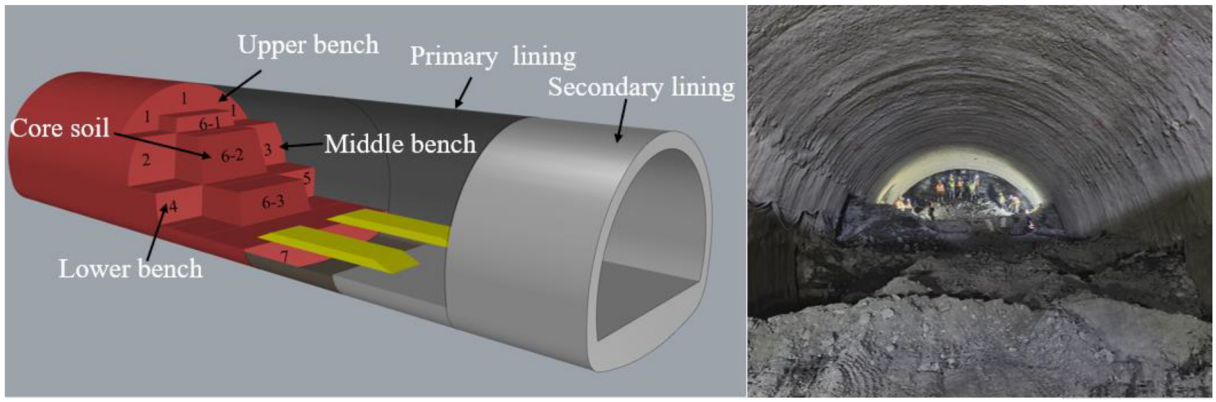

(a) Tunnel excavation method

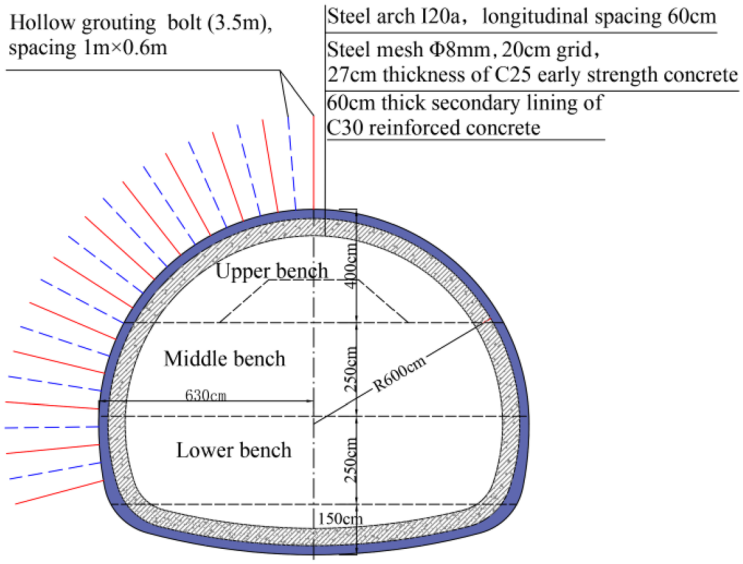

(b) Support form of tunnel

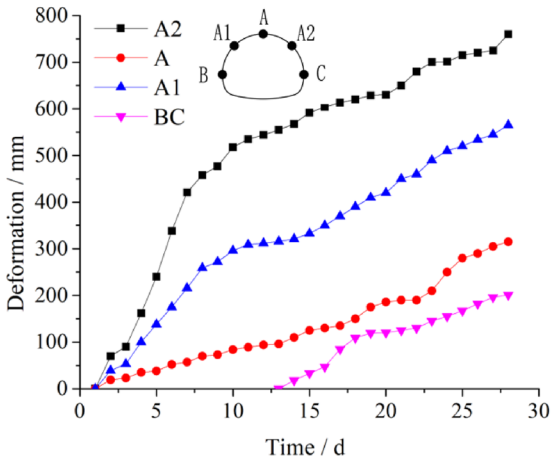

(c) Tunnel deformation monitoring

Fig. 6 Construction overview of the original tunnel support scheme

time exceeding 2 cm/d accounted for 41% of the time from the excavation step to the invert closure, and the maximum deformation exceeded more than 1 m. The section where the deformation exceeded 700 mm accounted for 60% of the total length. The steel arch replacement rate was more than 33%. Therefore, this scheme was not effective in controlling the deformation of the surrounding rock. The surrounding rock was mainly deformed asymmetrically, and the deformation on both sides was greater than that of the vault. In the severely deformed section, the broken surrounding rock was extruded from the primary support and collapsed. Even using a double-layer steel arch support could not effectively control the deformation. The failure characteristics of the primary support structure are shown in Fig. 7.

3 Analysis of the Deformation Mechanism of the Surrounding Rock

3.1 Rock Mechanics Tests

The MTS815.04 rock mechanics test system of the State Key Laboratory of Rock Mechanics and Geological Hazard Experimental Center was used for rock mechanics tests, as shown in Fig. 8. The experimental system is equipped with a variety of high-performance modules, which can accurately test the physical and mechanical characteristic parameters of the sample under various complex conditions. The stiffness of the reaction force frame of the equipment can reach 11.0 × 106 kN/m, the maximum axial force of 4600 kN can be applied, and the maximum confining pressure can reach 140 MPa.

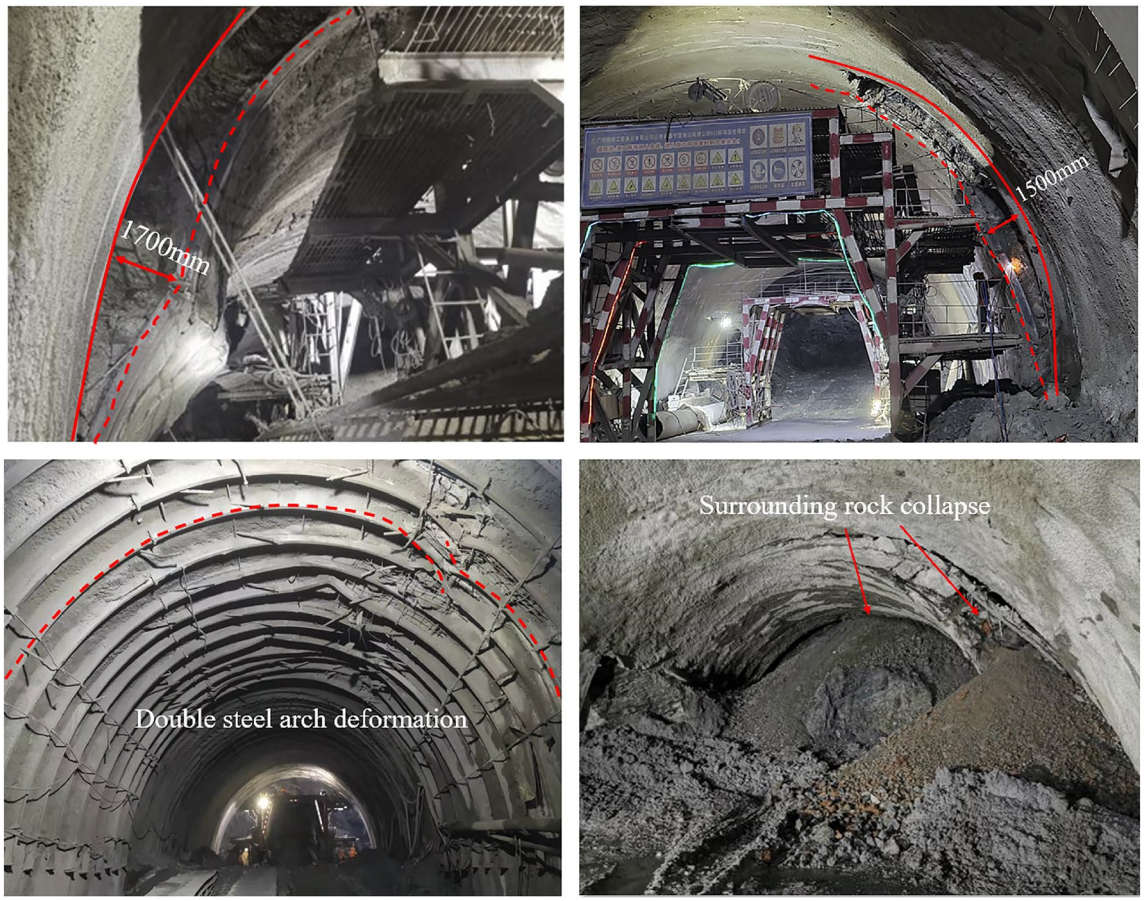

Fig. 7 Deformation of the initial support

Fig. 8 MTS experimental system

3.1.1 Tensile Strength Test (Split Test)

Rock samples with joint dips of 0°, 30°, 45°, 60°, and 90° were selected to test their tensile strength (Fig. 9a). The foliated structure of the rock mass is obvious. As shown in Fig. 9b, the failure of rock samples was mainly slip failure, and the failure of some rock samples was splitting failure. The experimental results are shown in Fig. 10. The tensile strength of the rock mass was between 2.14 and 3.67 MPa. With increasing joint dip, the tensile strength of the rock mass decreased gradually. The tensile strength was the smallest at 60° and rose at 90°.

3.1.2 Uniaxial Compression Test

To explore the influence of the joint dip angle on the rock mass strength, the angles of the prepared standard rock samples were 0°, 30°, 45°, 60°, 75°, and 90°. Photographs of some rock samples before and after the uniaxial compression test are shown in Fig. 11. The experimental results are shown in Fig. 12. The average uniaxial strength of the rock was between 18.2 and 51.2 MPa. The strength distribution of the rock samples at various dip angles shows that the strength of the rock samples at a fixed dip angle is relatively close. When the joint dip is 60°, the strength, elastic modulus, and Poisson's ratio of the rock sample are all the smallest, indicating that the rock sample has a larger axial strain during the experiment. When the dip angle is 0°, the uniaxial strength of the rock sample is the highest, with an average value of 51.7 MPa. The curve of uniaxial strength is U-shaped. Except for the fracture and failure of the rock sample at 0°, all other samples have slipped failure along the structural surface.

From the above rock mechanics test, it can be found that the structural plane of the rock mass is a weak part, and most of the samples slip between the rock layers under the action of the load. Therefore, after the surrounding rock is excavated, the sliding deformation between the rock layers will become dominant under the effect of ground stress.

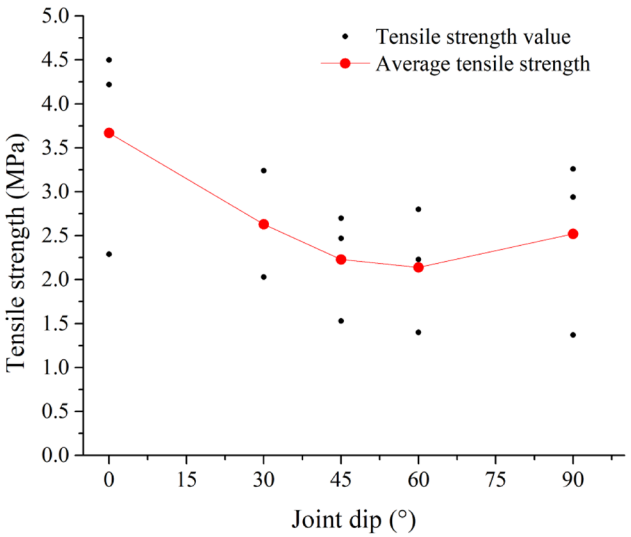

Fig. 10 Tensile strength test results

3.2 Numerical Simulation Analysis

3.2.1 Establishment of the Numerical Model

The tunnel numerical model was established using 3DEC based on the discrete element method to analyze the main causes of large deformation. The surrounding rock of the Changning Tunnel is layered with obvious cracks, and the thickness of the rock stratum is not uniform. To make the numerical model closer to the actual rock mass structure,

(a) Rock sample before experiment (b) Rock sample after test

Fig. 9 Photos before and after the failure of the rock sample

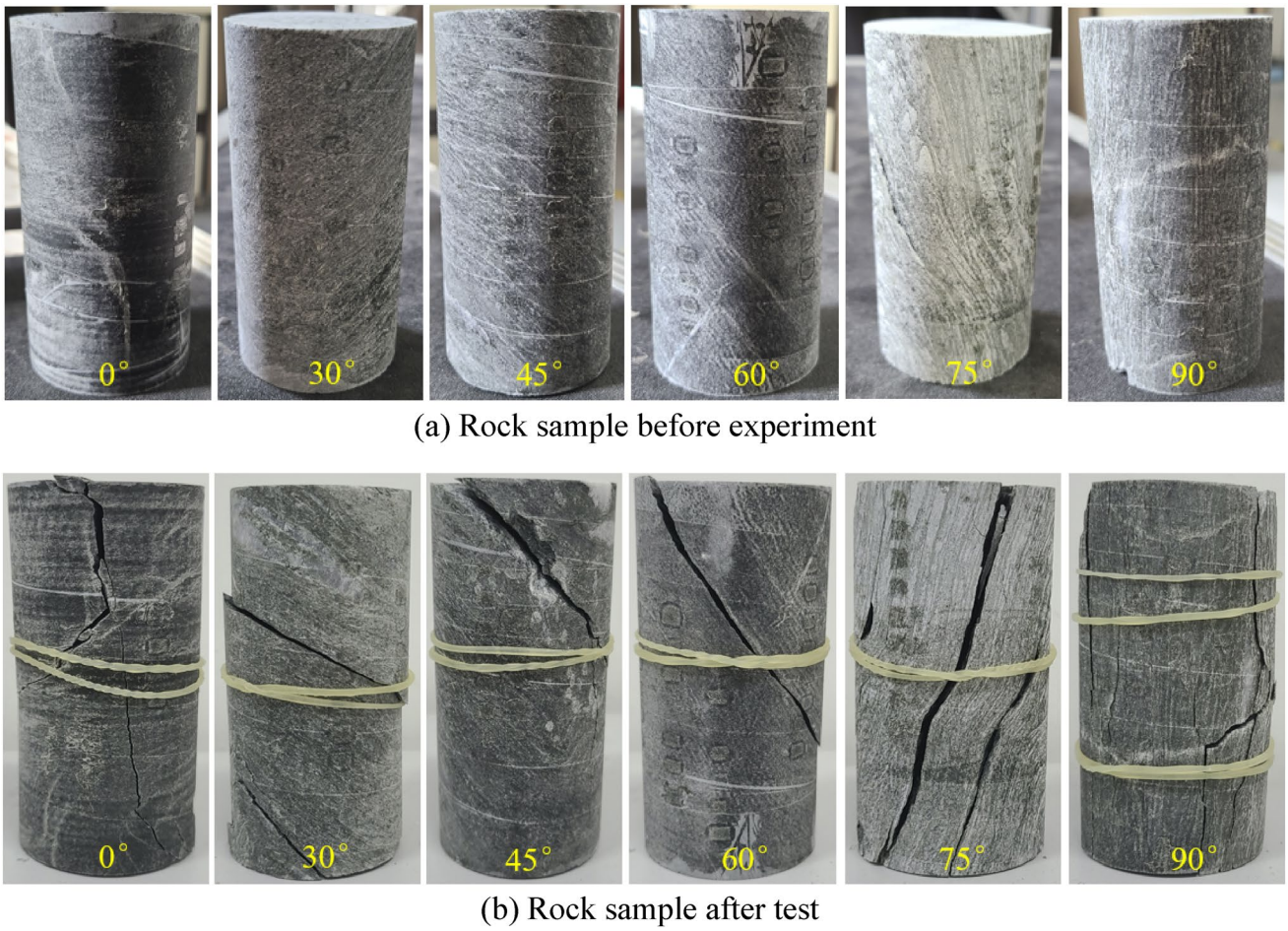

Fig. 11 Characteristics of rock samples before and after the uniaxial compression test

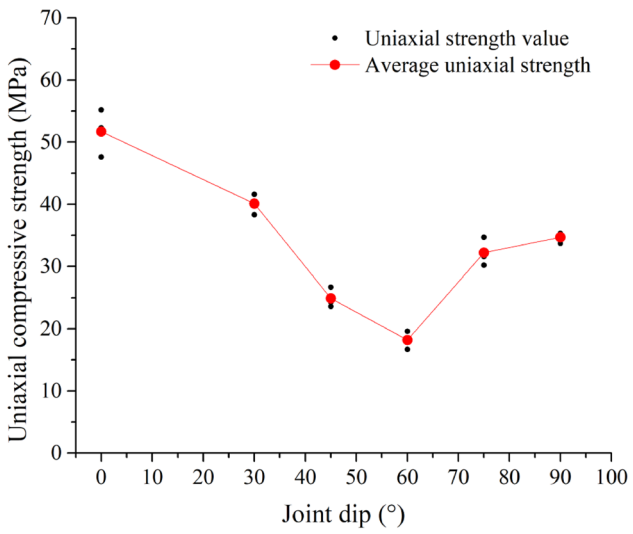

Fig. 12 Test results of the uniaxial compression test of the rock sample

tetrahedral blocks were first established to form the rock blocks of the surrounding rock, and then a discrete fracture network (DFN) was used to cut the blocks to form the rock structural plane. The discrete fracture joint model of a rock stratum with random thickness was established by this method. In the process of simulating the mechanical behavior of a rock mass, the rock mass was divided into two basic elements: a rock block and a joint. The joints are divided into dispersed joints and dominant joints. Dispersed joints simulate rock cracks after tunnel excavation, and dominant joints simulate the structural plane between rock strata. The Lagrangian solution method has natural advantages in solving the failure process of discontinuous media and is suitable for analyzing the large deformation or failure behavior of rock masses under dynamic and static loads. In this paper, the Hock–Brown constitutive model was used for rock blocks, and the Coulomb slip model was used for the joints (Fig. 13).

The model size is 50 m × 50 m × 1 m, the tunnel width is 12 m, and the height is 9 m, as shown in Fig. 13. The model is composed of 39,268 blocks with edges of 0.5–1 m

in length, and the rock stratum dip is 15° (Sun et al. 2019; Bahrani and Hadjigeorgiou 2018). Stress constraints were imposed on the left, right and upper parts of the model, and the bottom was fixed. According to geological data, the maximum principal stress is 15 MPa, the vertical stress is 8.5 MPa, and the minimum principal stress is 10 MPa. The maximum horizontal principal stress is parallel to the tunnel axis, and the minimum horizontal principal stress is perpendicular to the tunnel axis. Therefore, the stresses applied in the x, y, and z directions of the numerical model were 15 MPa, 10 MPa, and 8.5 MPa, respectively. First, the model runs to the equilibrium state to simulate the in situ stress state, and then the tunnel undergoes full section excavation to simulate the deformation mechanical characteristics of the surrounding rock without support.

3.2.2 Determination of Parameters

If the parameters of the numerical model are directly selected from the laboratory rock mass mechanics data, the calculation results may be quite different from the actual situation. The reason is that the rock samples obtained are often taken from relatively complete rock blocks on site, while most of the actual surrounding rock mass is broken rocks, and the measured rock mechanical parameters are high. Therefore, the mechanical parameters of the rock mass should be reduced according to the experimental data.

According to the uniaxial test results of the experiment, the uniaxial strength of the complete rock mass sample with 15° joints was approximately 45 MPa. The selection of parameters not only needs to consider the fixed attributes of rock, such as rock strength but also needs to be combined with the occurrence environment and structural characteristics of the rock mass. Hoek and Diederichs (2006) established a set of methods based on the GSI geological classification index and used the following formula for rock strength conversion:

$$\frac{E_{\mathrm{rm}}}{E_{\mathrm{i}}} = \left(0.02 + \frac{1 - D/2}{1 + \mathrm{e}^{(60+15D-\mathrm{GSI})/11)}}\right), \tag{1}$$

$$\sigma_{\mathrm{cmass}} = \sigma_{\mathrm{ci}} \frac{m_{\mathrm{b}} + 4s - a\left(m_{\mathrm{b}} - 8s\right)}{2(1+a)(2+a)} \left(\frac{m_{\mathrm{b}}}{4+s}\right)^{as-1}, \tag{2}$$

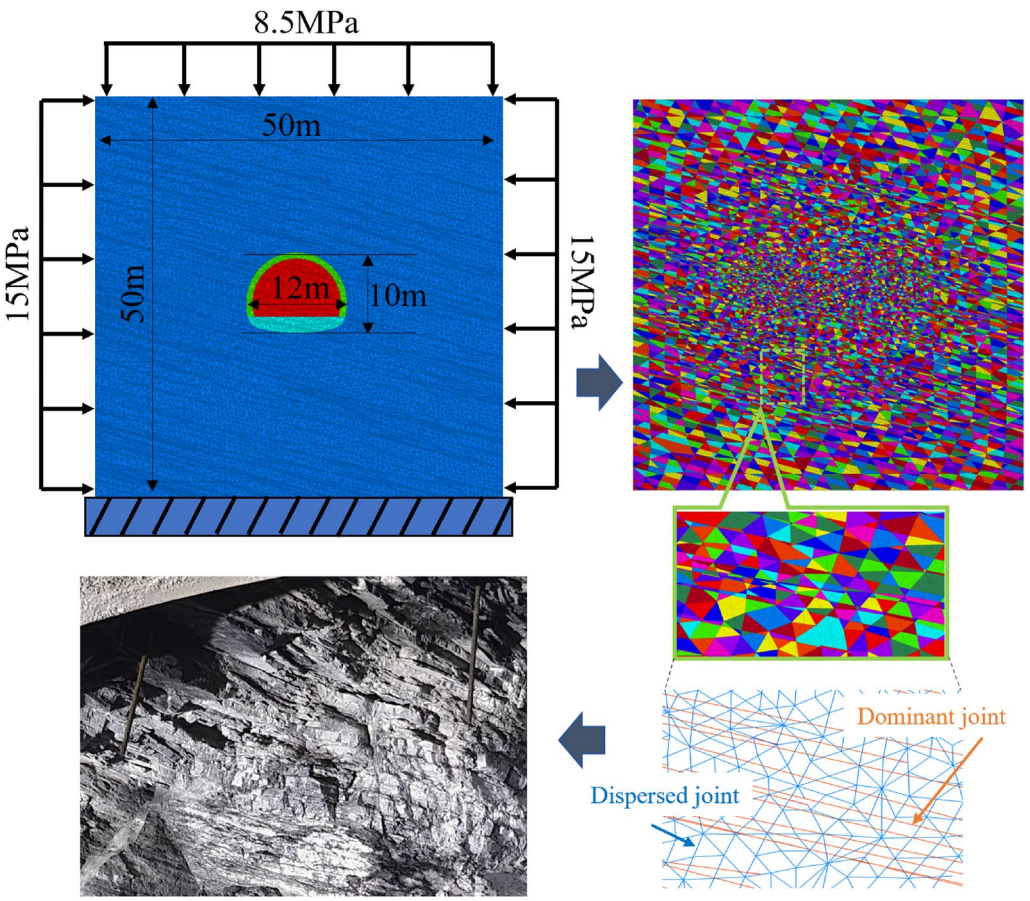

Fig. 13 Numerical model of the tunnel

Table 1 Rock mass parameters after the reduction calculation

Rock		Constant					Rock mass	
σ_{ci} (MPa)	E_i (GPa)	GSI	m_i	m_b	s	a	σ_{cmass} (MPa)	E_{rm} (GPa)
45	7.6	40	15	1.2	0.0006	0.511	6.4	0.5

Table 2 Mechanical parameters of the rock mass

Rock mass						Dispersed joint				
density (kg/m^3)	K (GPa)	G (GPa)	C^b (MPa)	φ^b	σ^b_t (MPa)	K_n (GPa)	k_s (GPa)	C^j (MPa)	φ^j	σ^j_t (MPa)
2500	0.27	0.21	1.1	22	0.5	8.5	3.42	2.7	29	2.4

$$m_b = m_i \exp\left(\frac{\mathrm{GSI}-100}{28-14D}\right), \tag{3}$$

$$S = \exp\left(\frac{\mathrm{GSI}-100}{9-3D}\right), \tag{4}$$

$$a = \frac{1}{2} + 1/6\left(e^{-\frac{\mathrm{GSI}}{15}} - e^{-\frac{20}{3}}\right), \tag{5}$$

where E_{rm} is the elastic modulus of the rock mass, σ_{cmass} is the uniaxial compressive strength of the rock mass, GSI is the geological strength index, E_i is the deformation modulus of the rock, and σ_{ci} is the uniaxial compressive strength of the intact rock. The parameter calculation formula follows Eqs. (1)–(9). The rock mass parameters obtained after calculation are shown in Tables 1 and 2. The dominant joint parameters of the rock mass were determined by numerical simulation inversion of uniaxial experiments, and the coupling method of the discrete fracture network and discrete element method (DFN–DEM coupling method) was used. After several inversions, it was determined that the index of the representative elementary volume (REV) of the model was 20 m × 10 m × 10 m. As shown in Fig. 14, after several uniaxial numerical simulations and inversion analyses, combined with the field-measured surrounding rock deformation data, *jkn* = 2e9, *jks* = 1e9, *jcoh* = 1e5, *jfr* = 25, and *jten* = 5e4 were selected as the dominant joint parameters.

$$K = \frac{E}{3(1-2\mu)} \tag{6}$$

$$G = \frac{E}{2(1+\mu)} \tag{7}$$

$$K_n = 10\left[\frac{K+\frac{3}{4}G}{\Delta z_{\min}}\right] \tag{8}$$

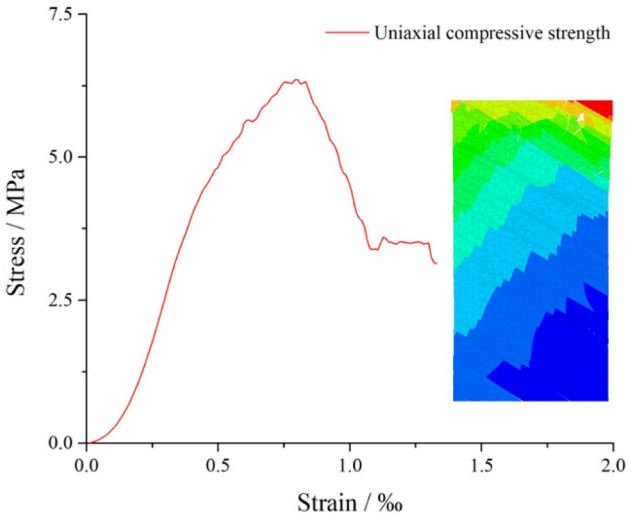

Fig. 14 Results of uniaxial numerical simulation of rock mass

$$K_s = 0.4K_n \tag{9}$$

3.2.3 Result Analysis

In the rock mechanics test, the structural surface of the rock mass is relatively smooth, and the rock mass is easily separated and slipped, which is more consistent with the numerical simulation results. As shown in Fig. 15a, separation and shear slip occurred on both shoulders of the tunnel, and the collapse after excavation was obvious. The deformation of the surrounding rocks on both sides will produce a greater pressure on the primary support, so the primary support vault is cracked and extruded. The plastic zone range of the surrounding rock presented a "+" shape, the failure of the surrounding rock was dominated by shearing. Only the shallow rock was damaged by tension. (Fig. 15b). The extension range of the plastic zone was approximately 0.9 times the tunnel span on the left and right sides, and the range of the plastic zone in the upper and lower parts of the

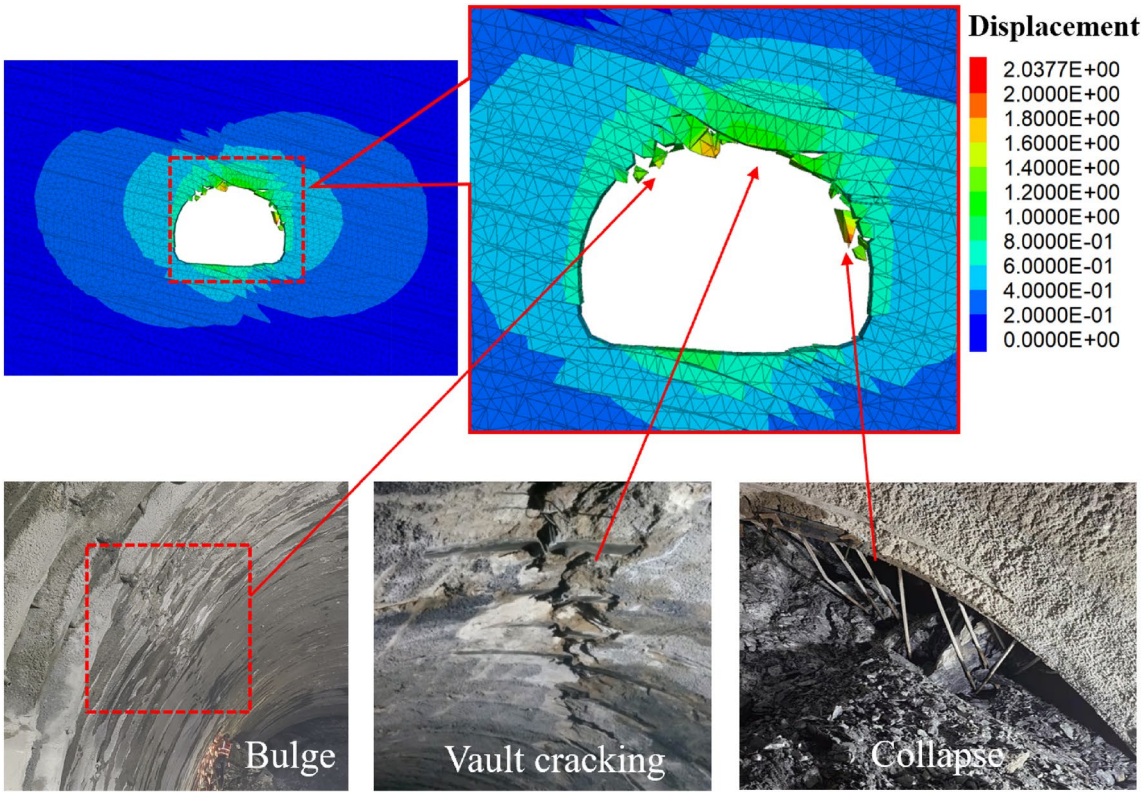

(a) Deformation characteristics of surrounding rock

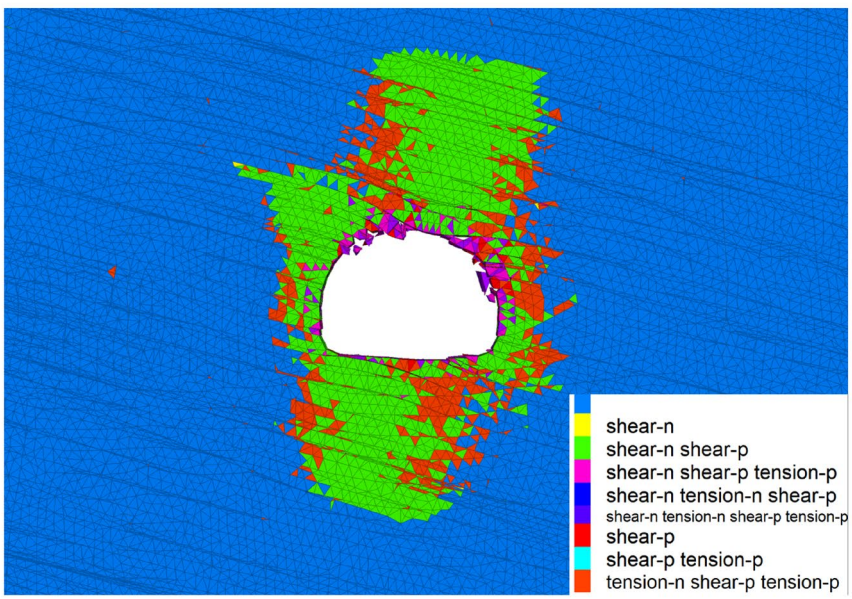

(b) Plastic zone

Fig. 15 Mechanical characteristics of the surrounding rock

tunnel exceeded the tunnel span. Figure 15c shows the core obtained on the right side of the tunnel. The rock is broken within 10 m (the tunnel span is 12 m), which is similar to the numerical simulation results. Due to the limitations of the coring-machine performance, the core depth can only be 10 m, which does not mean that under the ground support, the plastic zone of the surrounding rock is 10 m, which may be deeper. The failure of the tunnel support structure also

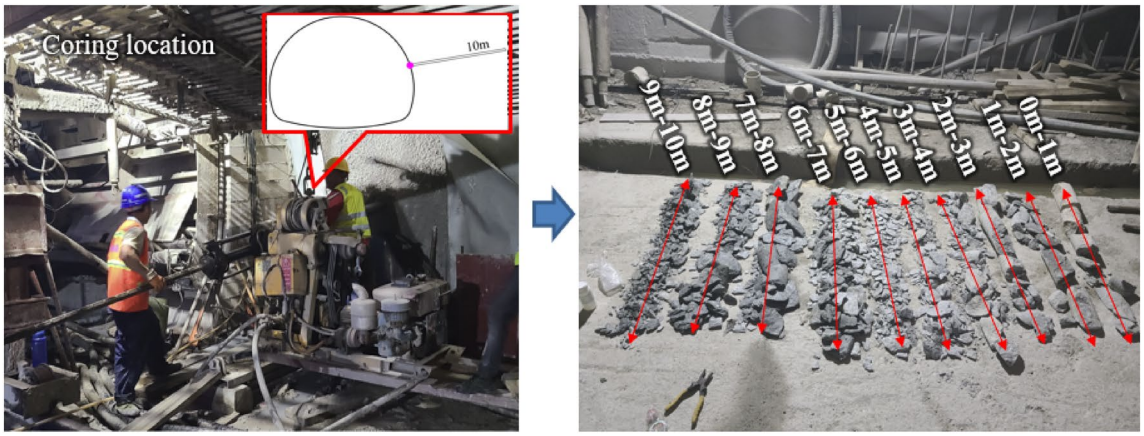

(c) Core obtained at ground support

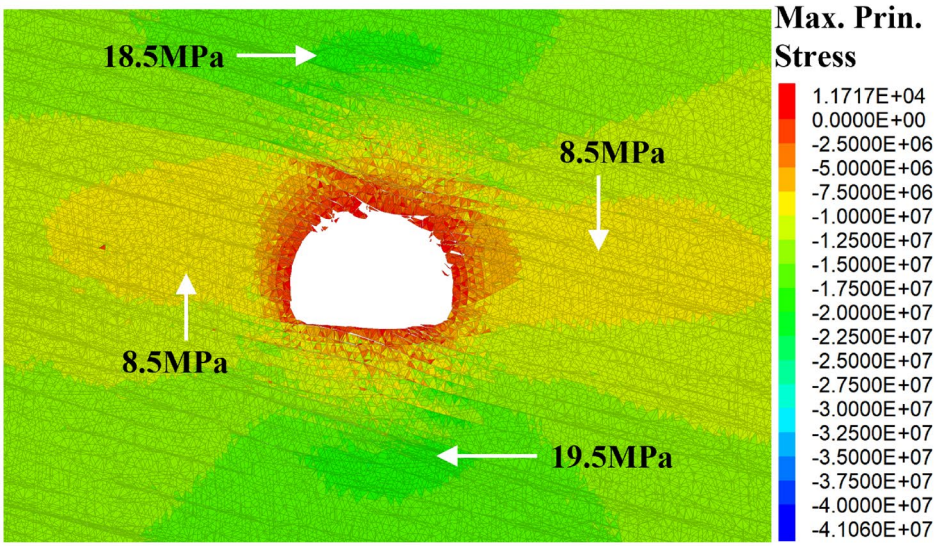

(d) Maximum stress

Fig. 15 (continued)

shows this point. A large number of broken rocks collapse, and the ground support cannot maintain the integrity and stability of the surrounding rock. The stress concentration area of the surrounding rock was mainly located in the vault and invert (Fig. 15d). The stress release area of the shallow surrounding rock tended to be consistent with the deformation range of the surrounding rock. Therefore, the active support method to improve the interlayer friction and the overall

strength of the surrounding rock has become the direction to solve the large deformation of the surrounding rock.

3.3 Mechanism Analysis of Large Deformation

Through the above analysis, the main causes of the large deformation of the Changning Tunnel are related to the tectonic stress, rock structure, and strength of the rock mass. The surrounding rock of the tunnel is layered, the rock mass strength is greatly affected by the rock structure, and the cohesion between rock layers is weak, so the rock layer will slip along the existing structural plane. Under the joint action of vertical stress and tectonic stress, coupled with the different values and directions of the two stress fields, the wedge-shaped blocks generated by the failure of the surrounding rock will appear randomly in different parts of the tunnel, resulting in large-scale or local deformation of the tunnel, as shown in Fig. 16a. After the tunnel is excavated, under the action of the initial stress field, the surrounding rock changes from the original three-dimensional stress state to a two-dimensional stress state, upsetting the stress balance of the surrounding rock. Under the stress field action, the normal direction of the rock stratum will be affected by the tangential stress, which will move the rock stratum toward the direction of the free face, cause the bending moment of the rock stratum, and easily cause the bending failure of the surrounding rock, as shown in Fig. 16b. According to the above research, the compression bending and shear sliding of rock strata caused by the rock structure and tectonic stress are the main reasons for the large deformation of the Changning Tunnel. The support shall be strengthened for the parts where that damage occurs.

4 NPR Anchor Cable Support Design

4.1 Composition and Characteristics of the NPR Anchor Cable

As shown in Fig. 17a, the negative Poisson's ratio anchor cable (NPR anchor cable) is composed of a constant resistance device, steel pallet, locking device, and anchor cable. The constant resistance device is composed of a cone body and casing pipe. According to the tensile curve (Fig. 17b), the deformation process of the NPR anchor cable is divided into three stages: the elastic tensile stage, constant resistance stage, and failure phase. The elastic stage refers to the stress of the NPR anchor cable not reaching the constant resistance value (350 kN), and the cable is elastically deformed under the influence of tension. The constant resistance stage means that when the force of the anchor cable reaches the allowable tensile stress (350 kN) of the constant resistance device, the cone body will slip in the casing pipe, resulting in a constant resistance sliding effect. In this process, the diameter of the cone body is larger than the inner diameter of the casing pipe, and the casing pipe expands with the extrusion of the cone body, resulting in a generalized negative Poisson's ratio effect. The failure stage means that the sliding distance of the cone body is close to the length of the casing pipe, and the cone body is gradually pulled out of the casing pipe. The test results showed that the constant resistance tensile distance of the NPR anchor cable is approximately 300 mm, and the average tensile force can reach 350 kN.

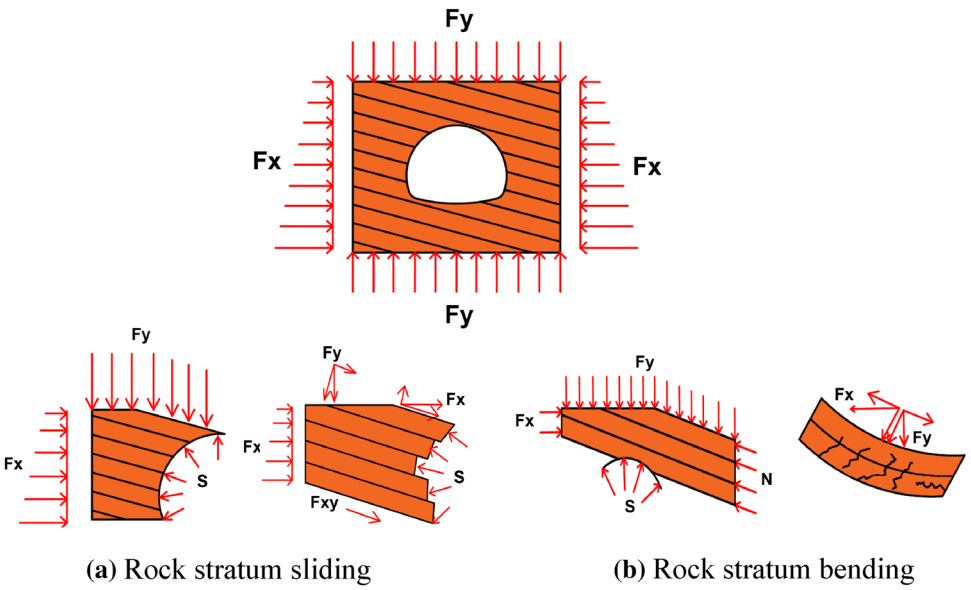

(a) Rock stratum sliding (b) Rock stratum bending

Fig. 16 Tunnel failure mode

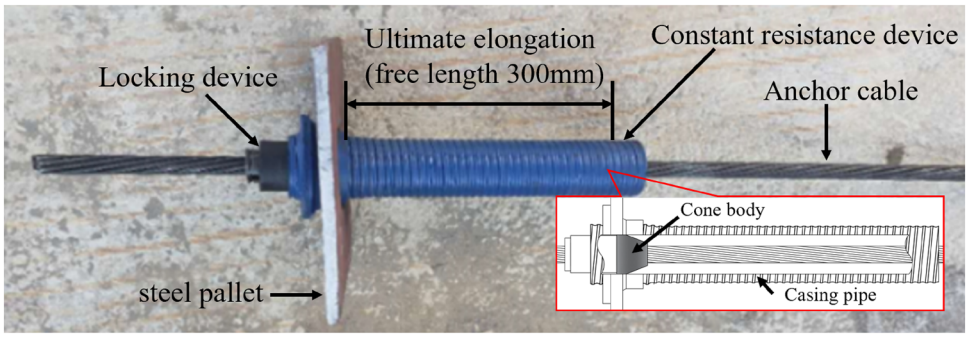

(a) Structure of NPR anchor cable

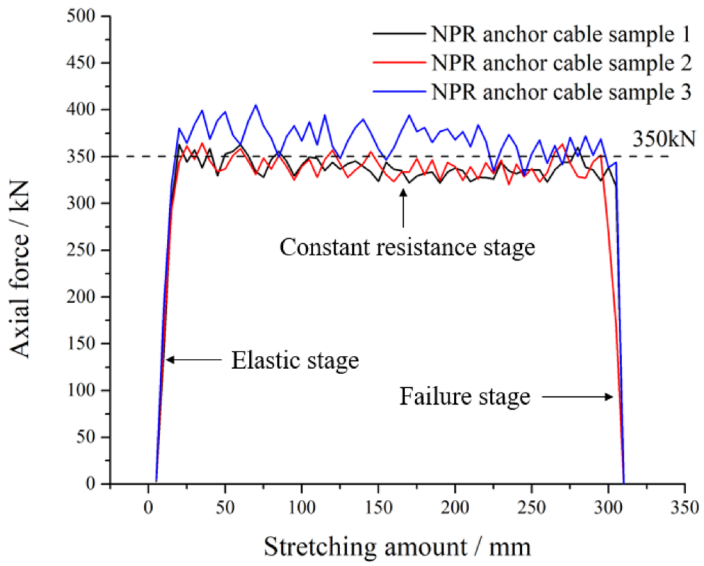

(b) NPR anchor cable tensile results

Fig. 17 Constant resistance and large deformation anchor cable

4.2 NPR Anchor Cable Support Principle

Traditional tunnel support measures cannot effectively control the large deformation of the surrounding rock, so a combined support form of "NPR long anchor cable + PR short anchor cable" is proposed, as shown in Fig. 18. The Poisson's ratio anchor cable (PR anchor cable) refers to the classic prestressed anchor cable (without the constant resistance device). This kind of support method was applied to tunnel engineering for the first time. After the PR short anchor cable is prestressed, it interacts with the shallow surrounding rock to form an arch structure. At the same time, the NPR long anchor cable can link the deep surrounding rock and form a double-layer arch structure with the shallow surrounding rock reinforced by the short anchor cable to actively strengthen the surrounding rock. Since the main component is an NPR long anchor cable, on the one hand, the mutual compression force is generated between the anchor cables in the surrounding rock with a large relaxation range, forming a compression arch (main compression arch), which greatly improves the stability of the surrounding rock.

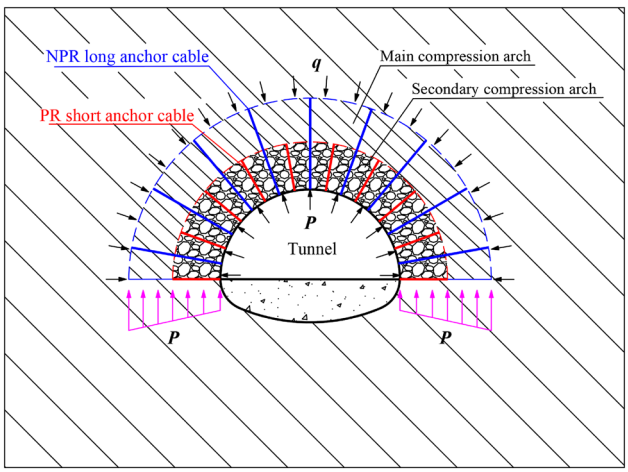

Fig. 18 Structure of the double-layer composite arch

On the other hand, the surrounding rock produces a shear force on the anchor cable, evenly transmits the tension to the anchor body and deep stable rock mass through the free

section, and provides sufficient anchoring force. Moreover, the secondary compression arch formed by the PR short anchor cable not only improves the stability of the surrounding rock over a large range but also bears a considerable part of the surrounding rock stress and reduces the load acting on the main compression arch. From an engineering point of view, the secondary compression arch formed by dense PR short anchor cables plays a decisive role in the long-term stability of the soft and weak surrounding rock.

Figure 19 shows that the prestressed NPR anchor cable can effectively strengthen the surrounding rock while allowing the surrounding rock to deform because the deformation of the surrounding rock can force the cone body in the casing pipe to slip. The constant resistance device can prevent the failure of the anchorage section of the anchor cable or the breaking of the anchor cable due to the deformation of the surrounding rock. Constant friction is generated in the process of cone body sliding to ensure that the anchoring force of the anchor cable satisfies the engineering requirements.

4.3 Support Scheme of NPR Anchor Cable

The support scheme of "NPR anchor cable + PR anchor cable + W-shaped steel strip + polyester fiber mesh" is shown in Fig. 20a. To solve the problem of large deformation of the Changning Tunnel, five support schemes were proposed. The difference between these support schemes is the number and length of NPR anchor cables. The support schemes are shown in Fig. 20b–f. The first scheme had the maximum support strength (Fig. 20b). The length of the NPR anchor cable was 10.3 m, and the length of the PR anchor cable was 6.3 m. The two kinds of anchor cables were installed alternately. In the second scheme (Fig. 20c), the row spacing of each type of anchor cable was increased from 1.2 to 1.6 m. The third scheme (Fig. 20d) reduced the length of the NPR anchor cable on both sides of the tunnel from 10.3 to 6.3 m, and the other parameters remained unchanged. The fourth scheme (Fig. 20e) increased the row spacing of each type of anchor cable to 2 m. The fifth scheme (Fig. 20f) removed the additional NPR long anchor cable at the left shoulder of the tunnel and then reduced the row spacing of each type of anchor cable to 1.6 m. The on-site support form of the NPR anchor cable is shown in Fig. 21. The detailed support parameters of each test section are shown in Table 3.

5 Field Test and Analysis

5.1 Field Monitoring Schemes

The test section is located at the exit of the right tunnel, with a mileage of K32 + 407–307, totaling 100 m. The 100 m test section is further divided into five small test sections, each of which is 20 m. An NPR anchor cable support scheme should be applied to each small test section. Each small test section has a monitoring station located in the middle, at K32 + 397, K32 + 377, K32 + 357, K32 + 337, and K32 + 317, as shown in Fig. 22. The monitoring data include primary support deformation, pressure between the primary support and surrounding rock, pressure between the primary and secondary

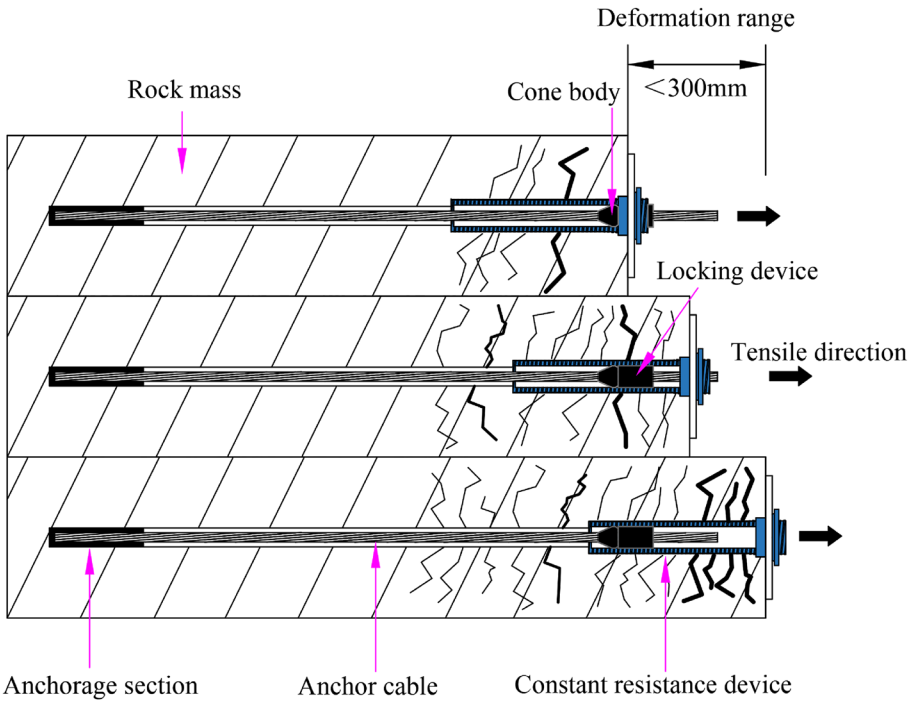

Fig. 19 Interaction between the NPR anchor cable and the surrounding rock

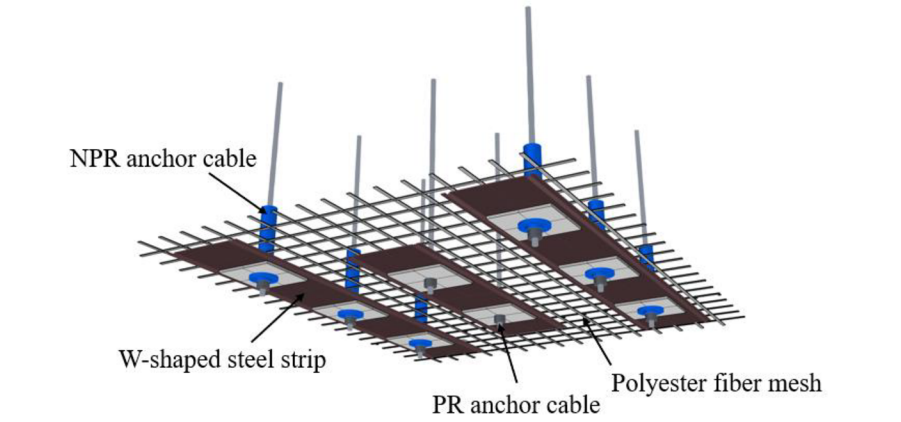

(a) NPR anchor cable + PR anchor cable support form

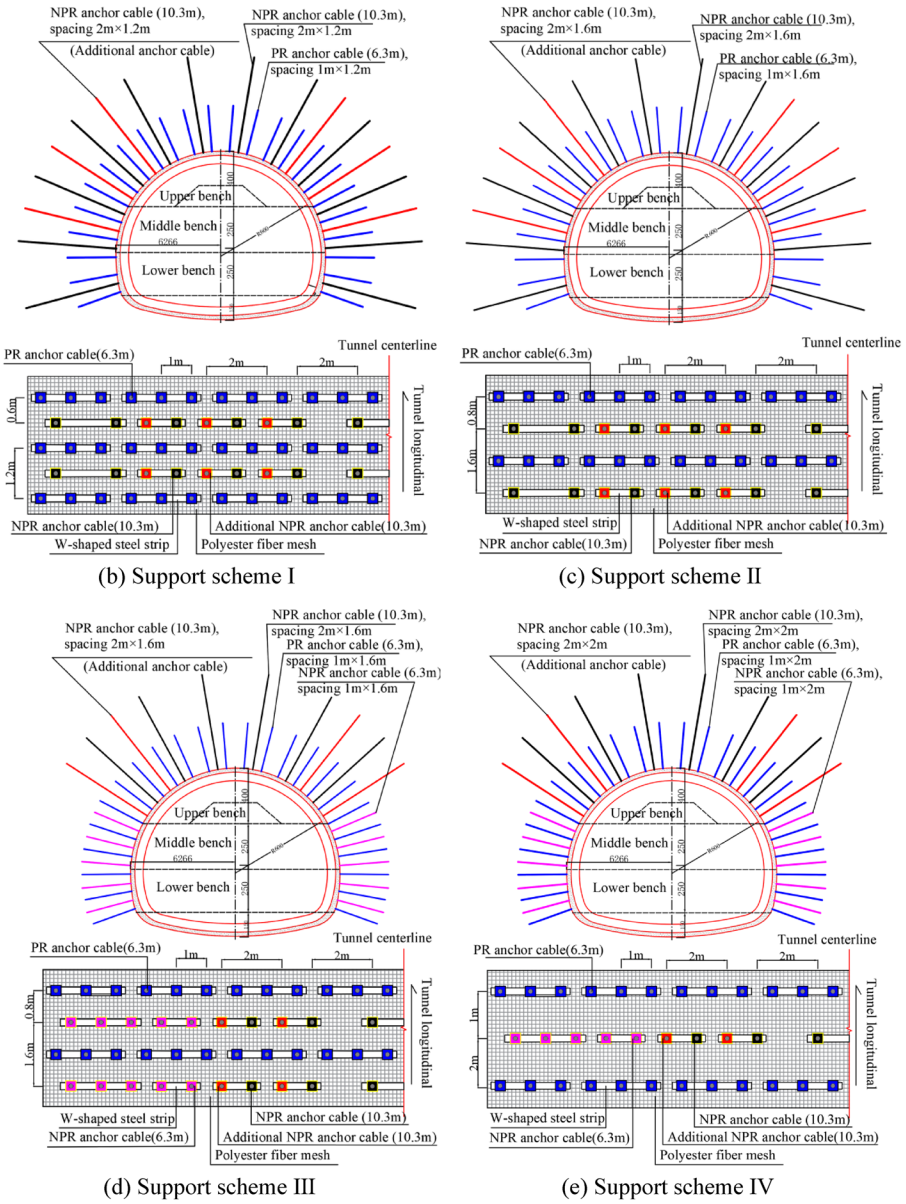

Fig. 20 (continued)

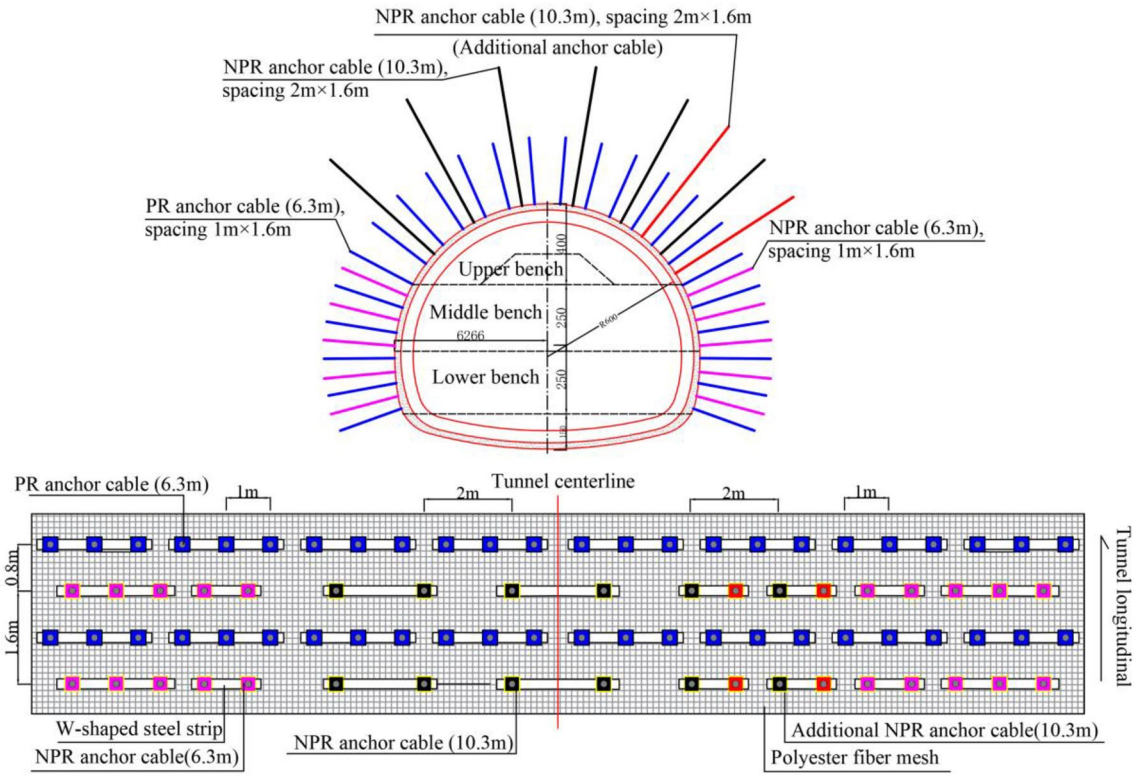

(f) Support scheme V

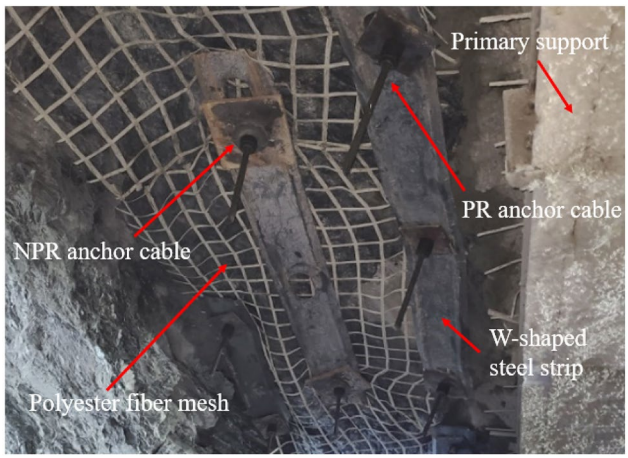

Fig. 21 Schematic diagram of test section support

lining, internal stress of the steel arch, axial force of the NPR anchor cable, and deep displacement of the surrounding rock. The monitoring equipment is shown in Fig. 23, which includes pressure axial force gauges, pressure gauges, stress gauges, and displacement gauges. The data acquisition box can automatically collect relevant monitoring data for long-term monitoring. The axial force gauge is used to monitor the axial force change of the NPR anchor cable. The pressure gauge is used to monitor the pressure between the surrounding rock and primary support, as well as the pressure between the primary support and secondary lining. The stress gauge is used to monitor the internal stress of the steel arch support, and the multipoint displacement gauge is used to monitor the displacement of the deep surrounding rock. Each monitoring station has 5 monitoring points located on the vault, left and right waist, and left and right shoulders. The installation of the multipoint displacement meter was complex, so only one was installed in each monitoring section. The monitoring frequency was once per day. The sensor placement is shown in Fig. 24.

5.2 Safety Criteria

The safety assessment of the tunnel lining in this paper should be based on the mechanical response considering internal stress, pressure and displacement. By comparing the monitoring data with material strength and allowable deformation, the safety of the tunnel lining can be directly assessed. Table 4 shows safety standards according to Code for Design on Tunnel of Railway (TB 10003-2016 2016), Technical Specification for Monitoring Measurement of Railway Tunnel (Q/CR 9218-2015 2015), and Specifications for Design of Highway Tunnels (JTG 3370.1-2018 2018) in China. The strength-based safety factor is the critical

Table 3 Main support parameters of five schemes

Items	Support scheme I	Support scheme II	Support scheme III	Support scheme IV	Support scheme V
Scope of test section	K32 + 407–387	K32 + 387–367	K32 + 367–347	K32 + 347–327	K32 + 327–307
Reserved deformation	650 mm	500 mm	350 mm	350 mm	350 mm
Excavation length	1.2 m/day	1.6 m/day	1.6 m/day	2.0 m/day	1.6 m/day
prestress	> 300 kN	> 300 kN	> 300 kN	> 300 kN	> 300 kN
Anchoring force	350 kN	350 kN	350 kN	350 kN	350 kN
NPR anchor cable	Φ21.8, L = 10.3 m	Φ21.8, L = 10.3 m	Φ21.8, L = 10.3 m Φ21.8, L = 6.3 m	Φ21.8, L = 10.3 m Φ21.8, L = 6.3 m	Φ21.8, L = 10.3 m Φ21.8, L = 6.3 m
PR anchor cable	Φ21.8, L = 6.3 m	Φ21.8, L = 6.3 m	Φ21.8, L = 6.3 m	Φ21.8, L = 6.3 m	Φ21.8, L = 6.3 m
Steel rib	I20a@60 cm	I20a@80 cm	I20a@60 cm	I20a@60 cm	I20a@60 cm
Shotcrete	C25, T = 27 cm	C25, T = 15 cm	C25, T = 15 cm	C25, T = 15 cm	C25, T = 15 cm
W-shaped steel strip	2200 mm × 300 mm × 2.8 mm	2200 mm × 300 mm × 2.8 mm	2200 mm × 300 mm × 2.8 mm	2200 mm × 300 mm × 2.8 mm	2200 mm × 300 mm × 2.8 mm
Steel mesh	φ8 × 20 cm × 20 cm	φ8 × 20 cm × 20 cm	φ8 × 20 cm × 20 cm	φ8 × 20 cm × 20 cm	φ8 × 20 cm × 20 cm
Polyester fiber mesh	100 mm × 100 mm	100 mm × 100 mm	100 mm × 100 mm	100 mm × 100 mm	100 mm × 100 mm
Reinforced concrete	C30, T = 60 cm	C30, T = 50 cm	C30, T = 50 cm	C30, T = 50 cm	C30, T = 50 cm

parameter to evaluate the construction risk, as defined by Eq. (10). The safety of the secondary lining is indirectly reflected by referring to the sharing proportion of the primary support and secondary lining compression, as defined by Eq. (11).

$$\text{Safety factor} = \frac{\text{Standard strength of supporting structure}}{\text{Measured stress of supporting structure}} \tag{10}$$

$$\text{Second lining load sharing ratio} = \frac{\text{Pressure on the second lining}}{\text{Pressure on the primary support}} \times 100\% \tag{11}$$

5.3 Monitoring Results and Analysis

5.3.1 Deformation Behaviors

Figure 25a shows the maximum displacement of each monitoring section. The NPR anchor cable support strength of Support scheme I was the highest, and the surrounding rock deformation was the smallest. The maximum deformation of this section was 38 mm. With the decrease in the number of NPR anchor cables in each scheme, the displacement of the surrounding rock gradually increases. The maximum deformation was 135 mm, which appeared in Support scheme IV, but it was still less than the standard 190 mm in the specification. The deformation rates of different schemes are recorded in Fig. 25b. The deformation of the surrounding rock was divided into two stages. Before the excavation of the lower bench, the surrounding rock was in the rapid deformation stage, and the maximum deformation rate was 21 mm/day. After the excavation of the lower bench, the deformation rate of the surrounding rock gradually decreased to 0 mm/day and changed to a stable stage. The deformation of the surrounding rock was basically stable within approximately 25 days.

5.3.2 Internal Stress of Steel Arch

Figure 26a shows the maximum value of the internal stress of the steel arch in each monitoring section. In the monitoring results, the value is positive under tensile stress and negative under compressive stress. In the whole process of excavation and support, the steel arch was tensioned first and then gradually changed to the compression state. After the excavation of the lower bench, the internal stress of the steel arch gradually decreased in a stable process. The results show that the closure of the primary support is beneficial in reducing the internal stress of the steel arch and improving its safety. According to Eq. (10), the standard axial strength is compared with the maximum internal stress value of the

steel arch in each monitoring section; the results are shown in Fig. 26b. The safety factor of the primary support in each support section is greater than 1, and the maximum value of the internal stress of the steel arch (280 MPa) is within the standard range (335 MPa). The results show that the primary support structure is relatively safe.

5.3.3 Deep Multipoint Displacement

The sensor installation depth was located at 1 m, 6 m, and 10 m away from the free face to observe the displacement of the surrounding rock within the length range of the anchor cable. Select the monitoring results of Support schemes IV, as shown in Fig. 27, the displacement of the 10 m measuring points was small, but the displacement of the 1 m and 6 m measuring points was large. Therefore, the displacement of the surrounding rock was concentrated in the shallow part, and the surrounding rock at 10 m depth was basically stable. The surrounding rock displacement trend covered by the PR short anchor cable (6 m) was consistent, while the surrounding rock displacement change covered by NPR long anchor cable (10 m) was small. This showed that the PR short anchor cable support formed the shallow rock arch structure and had overall displacement, and the NPR long anchor cable formed the second stable rock arch structure and limited the displacement of the shallow arch structure, ensuring the stability of deep surrounding rock.

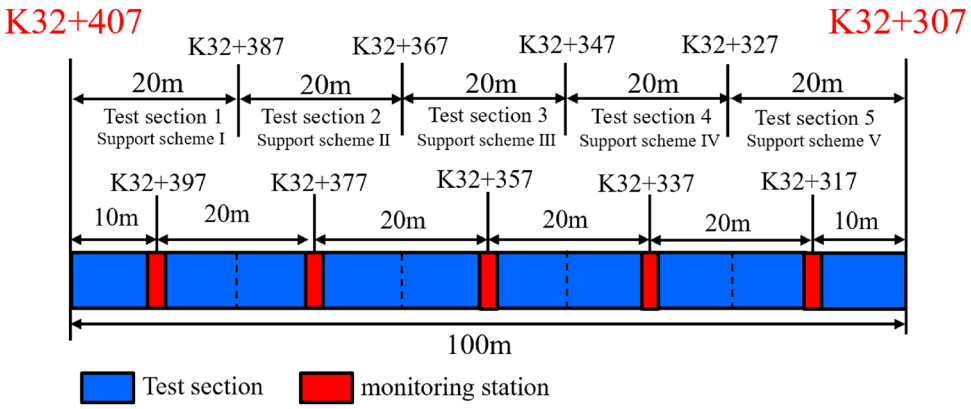

Fig. 22 Location of the tunnel monitoring station and test section

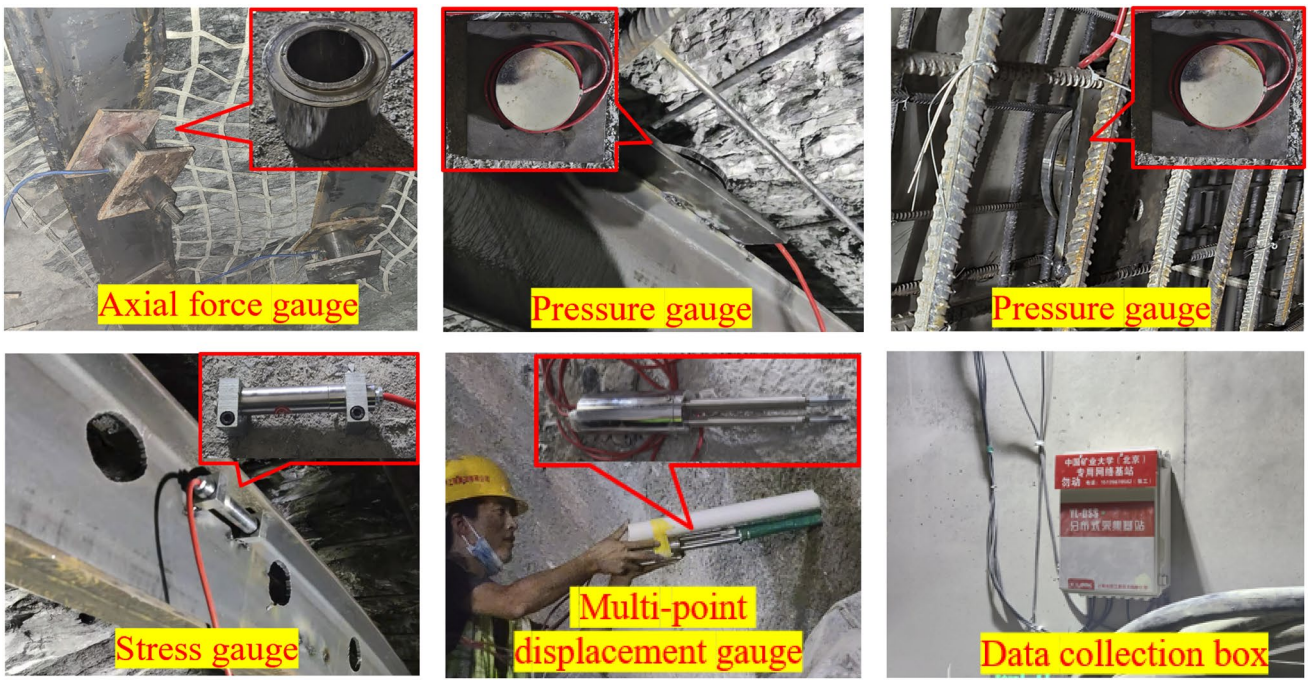

Fig. 23 Tunnel monitoring equipment

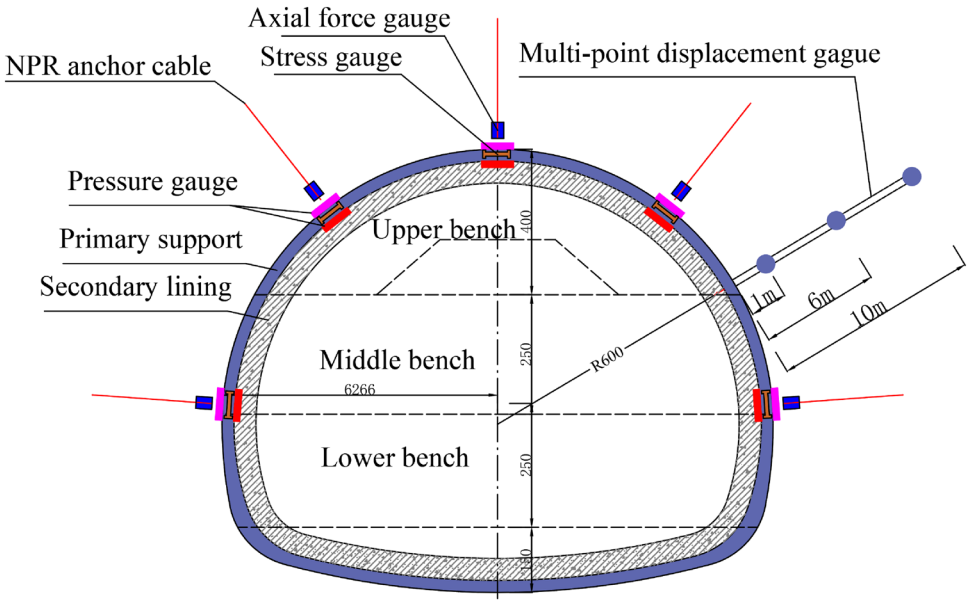

Fig. 24 Measuring points of the monitoring station

5.3.4 Primary Support Pressure and Secondary Lining

Table 4 Chinese standards of tunnel displacement and internal stress in support structures

Rock mass grade	Tunnel displacement (mm)	Standard axial compressive/ tensile strength of steel frame (MPa)	Proportion of secondary lining load
V	190	335	60–80%

Figure 28a and b records the pressure value change trend of the maximum pressure measuring point of each monitoring station. As shown in Fig. 28a, the pressure between the primary support and surrounding rock was basically consistent with the change trend of the surrounding rock displacement, which was also divided into a rapid growth stage and a stable stage. As shown in Fig. 28b, after the construction of the secondary lining, the pressure between the primary support and the secondary lining increased rapidly during the 14-day curing period, and then the pressure growth rate slowed down. After 28 days, the concrete strength reached the maximum value, and the pressure on the secondary lining gradually stabilized. According to Eq. (11), the final

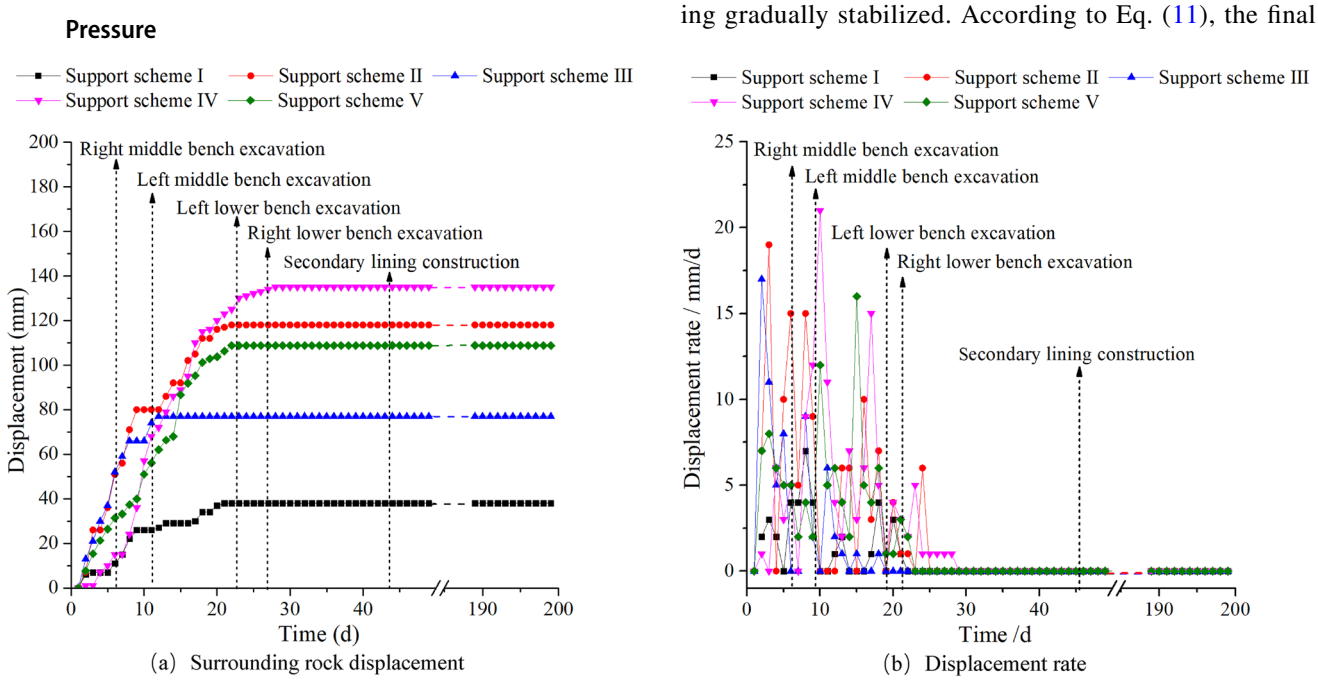

Fig. 25 Displacement of the primary support

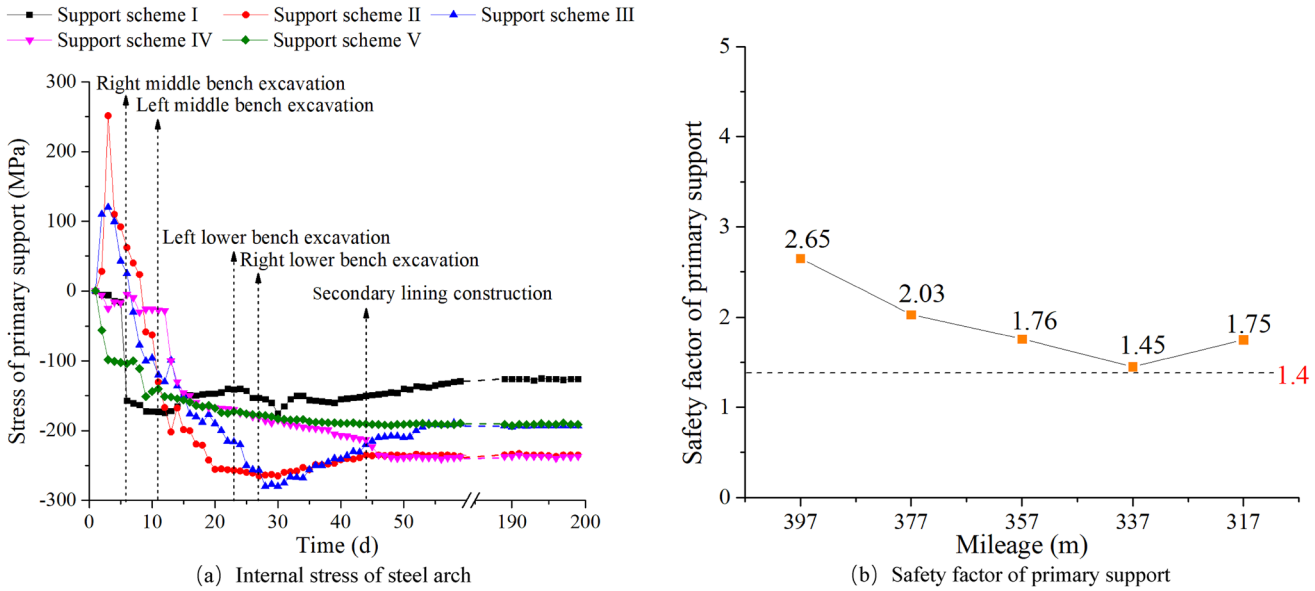

Fig. 26 Internal stress monitoring results of the primary support

monitoring results of the two pressures are compared to determine the load proportion of the secondary lining, and the results are shown in Fig. 28c. The results showed that the load proportion of the secondary lining was between 8.1 and 14.1%, which was less than the range recommended by the standard (60–80%). The pressure borne by the secondary lining was small, and the pressure was mainly borne by the primary support. Therefore, the secondary lining participates in tunnel support as a basic safety reserve.

5.3.5 Axial Force of Anchor Cable

Figure 29 records the axial force change of the NPR anchor cable at the maximum displacement at each monitoring station. After more than 300 kN of prestress was applied to the anchor cable and before the initial support was closed, the axial force of the NPR anchor cable first increased, then decreased, and finally tended to be stable. In the stable stage, the axial force of the anchor cable was approximately 350 kN, reaching a constant resistance value, which showed that the NPR anchor cable plays a high prestressed constant resistance role in places with large displacements.

5.3.6 Reserve Deformation of the Surrounding Rock

The reserved deformation of the tunnel is an important guarantee for controlling the deformation of the surrounding rock without intrusion, and it also affects the construction cost of the tunnel. Therefore, each support scheme must consider these two factors and determine a reasonably reserved

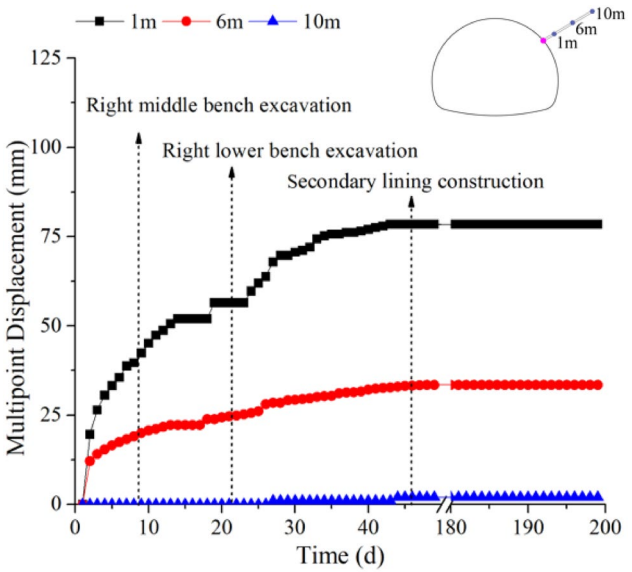

Fig. 27 Deep displacement of the surrounding rock

deformation of the surrounding rock. Figure 30 records the reserved deformation of the tunnel design and the remaining minimum reserved deformation. Under the five NPR anchor cable tunnel support schemes, the reserved deformation and the remaining reserved deformation show a positive correlation trend. Fitting the difference between the two, the difference curve gradually becomes stable from large to small. The average value of the difference between the five test sections is approximately 210 mm. The maximum deformation

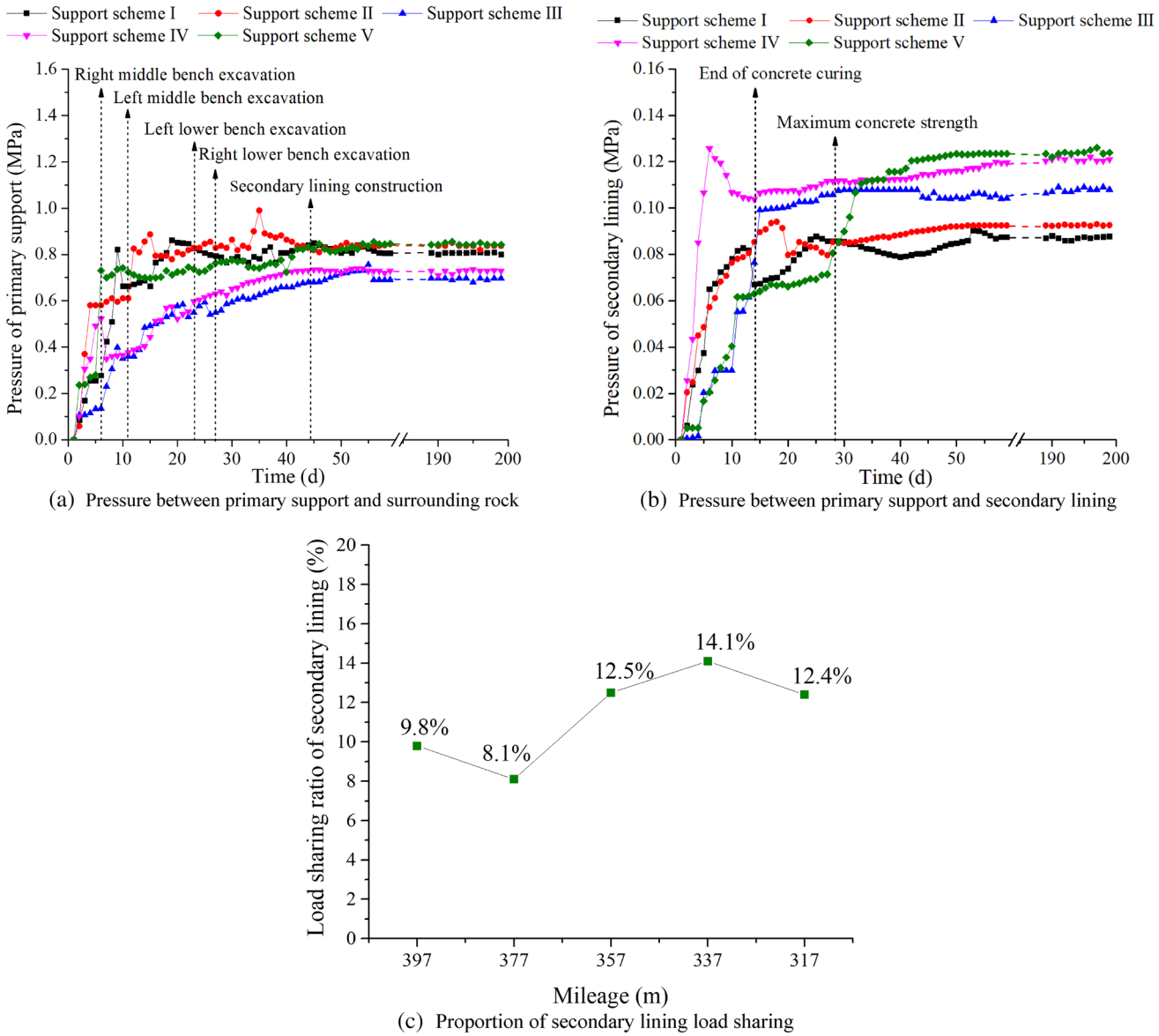

Fig. 28 Pressure monitoring results of the supporting structure

of the surrounding rock in the test section of 135 mm can be added to the difference, and the obtained 345 mm is basically consistent with the design value (350 mm). This value can be used as the minimum reserved deformation of the tunnel and provides a reference for the determination of the reserved deformation of the subsequent tunnel construction.

5.4 Support Effect

Based on the above monitoring results, when the tunnel used Support scheme V with the least number of NPR anchor cables, the monitoring data of the surrounding rock are within the controllable range, and the safety of the primary support and secondary lining can be effectively guaranteed. Therefore, Support scheme V is the best. After adopting the support scheme, the support effect is shown in Fig. 31. At the boundary between the test section and the nontest section, the concrete on the vault of the nontest section cracked and fell off, and the initial support structure of the test section was intact, indicating that the NPR anchor cable can effectively control the stability of the surrounding rock.

6 Conclusion

The Changning Tunnel construction process was seriously affected by the large soft rock deformation. The deformation characteristics of the tunnel were analyzed in this paper, and

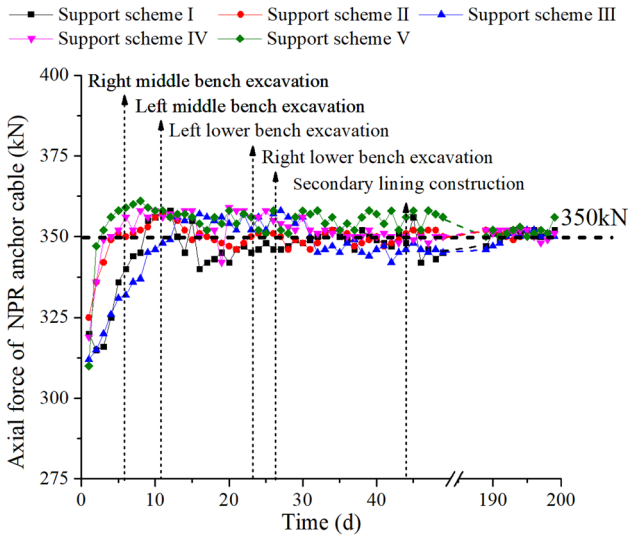

Fig. 29 Axial force NPR anchor cable

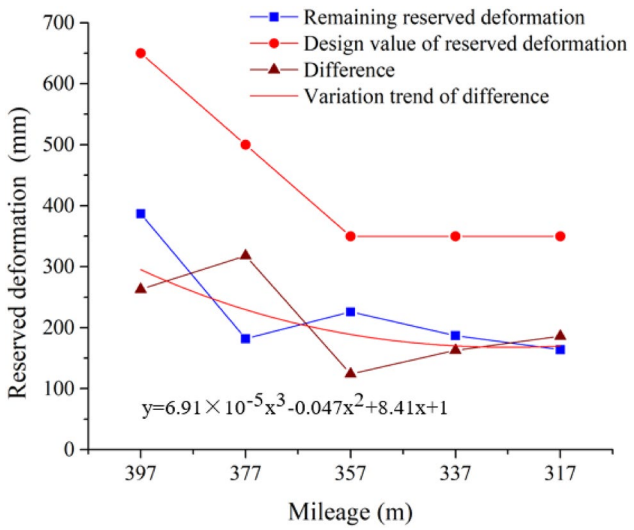

Fig. 30 Reserved deformation of the tunnel

the deformation mechanism of the surrounding rock was analyzed by laboratory rock mechanical tests and numerical simulations. Field tests were used on the 5 NPR anchor cable support schemes, and the support effects were analyzed through on-site monitoring. The main conclusions drawn are as follows.

1. The Changning Tunnel is a typical jointed soft rock tunnel. Under different joint dips, the strength distribution of the rock stratum is discrete. The failure characteristics of the rock mass are mainly a sliding failure of the structural plane. Under the tectonic stress action, low-strength rock masses are prone to plastic failure, resulting in large deformation of the primary support. The field investigation, numerical analysis, and laboratory test indicate that rock strata compression bending and shear slip caused by the rock strata structure and tectonic stress are the main causes of large deformation in the Changning Tunnel.
2. The large deformation of the Changning Tunnel is uncontrollable under conventional support measures. The NPR anchor cable exhibited the advantages of high constant resistance (350 kN) and large tensile capacity (300 mm). The NPR anchor cable and the PR anchor cable can actively strengthen the surrounding rock together to form a double-layer reinforced arch structure. The prestressed dense PR short anchor cables reinforced the shallow surrounding rock and reduced the shear slip tendency between rock layers. The high prestressed NPR long anchor cables could adaptively adjust the deformation of the surrounding rock while further strengthening the surrounding rock and controlling the deformation of the surrounding rock within 300 mm.
3. Five support schemes of "NPR anchor cable + PR anchor cable" were tested in the field. The NPR anchor cable was installed alternately with a length of 10.3 m, and the PR anchor cable was installed alternately with a length of 6.3 m. The number of NPR anchor cables was different in each of the five schemes, but these support schemes can control the deformation of the surrounding rock to varying degrees. The maximum deformation of the Changning Tunnel was less than 150 mm. After the excavation of the working face, the surrounding rock deformation converged within 25 days. After the construction of the NPR anchor cable, the contact pressure between the primary lining and surrounding rock and the contact pressure between the primary lining and the secondary lining were far less than the maximum bearing capacity of the structure. The research results can provide a reference for the prevention and control of large deformation in similar projects.

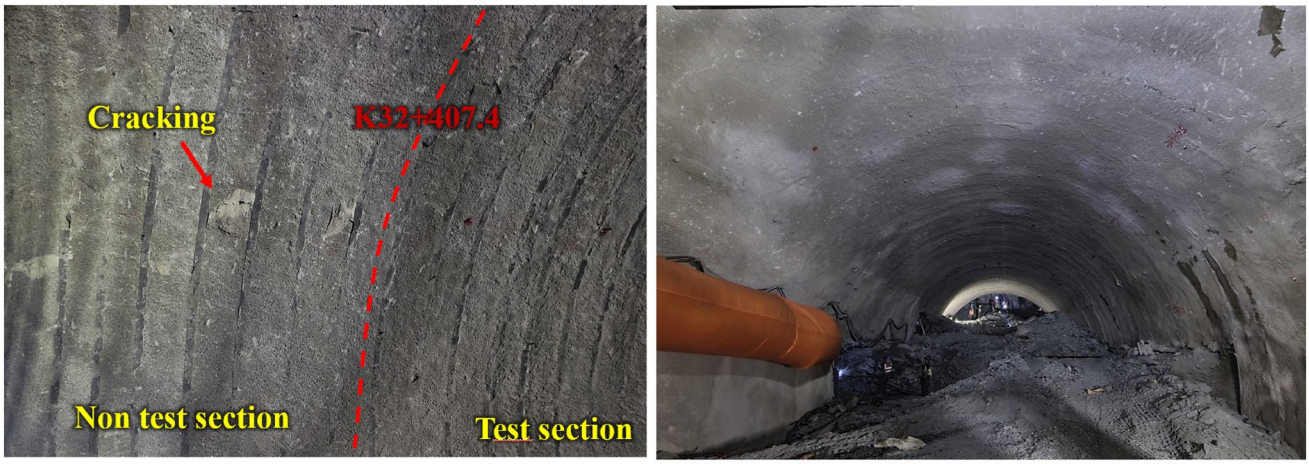

(a) Boundary between test section and non-test section

(b) Overall view of test section

Fig. 31 Support effect of the NPR anchor cable

Acknowledgements This work was supported by the National Natural Science Foundation of China (Grant No. 41941018).

References

Anagnostou G (1993) A model for swelling rock in tunnelling. Rock Mech Rock Eng 26(4):307–331

Ang N et al (2018) Stability analysis and failure mechanism of the steeply inclined bedded rock masses surrounding a large underground opening. Tunn Undergr Space Technol 77(1):45–58

Aydin A, Ozbek A, Cobanoglu I (2004) Tunnelling in difficult ground: a case study from Dranaz tunnel, Sinop, Turkey. Eng Geol 74(3–4):293–301

Aygar EB (2020) Evaluation of new Austrian tunnelling method applied to Bolu tunnel's weak rocks. J Rock Mech Geotech Eng 12(3):541–556

Bahrani N, Hadjigeorgiou J (2018) Influence of stope excavation on drift convergence and support behavior: insights from 3D continuum and discontinuum models. Rock Mech Rock Eng 51:2395–2413

Bao LH (2014) In situ stress measurement and surrounding rock stability analysis of the Gaoligong mountain tunnel. Appl Mech Mater 501–504:1766–1773

Bonini M, Barla G (2012) The Saint Martin La Porte access adit (Lyon-Turin Base Tunnel) revisited. Tunn Undergr Space Technol 30:38–54

Bosman JD, Malan DF, Drescher K (2000) Time-dependent tunnel deformation at Hartebeesfontein Mine. J S Afr Inst Min Metall 100(6):333–340

Brox D, Hagedorn H (1999) Extreme deformation and damage during the construction of large tunnels. Tunn Undergr Space Technol Inc Trenchless Technol Res 14(1):23–28

Cao C, Zhang W, Chen JP et al (2021) Quantitative estimation of debris flow source materials by integrating multi-source data: a case study. Eng Geol 291:106222

Chen ZM, Zhao DA, Yu YY (2011) The interaction mechanism of surrounding rock and supporting structure in high geostress extrusion fault. Adv Mater Res 243–249:3588–3598

Chen J, Liu W, Chen L et al (2020) Failure mechanisms and modes of tunnels in monoclinic and soft-hard interbedded rocks: a case study. KSCE J Civ Eng 24(4):1357–1373

Chen DH, Chen HE, Zhang W et al (2022) An analytical solution of equivalent elastic modulus considering confining stress and its variables sensitivity analysis for fractured rock masses. J Rock Mech Geotech Eng 14(3):825–836. https://doi.org/10.1016/j.jrmge.2021.08.007

Cui G, Qi J, Wang D (2020) Research on large deformation control technology of tunnels in squeezing rock and its application. Sci Prog 103(2):36850420923167

Dalgıç S (2002) Tunneling in squeezing rock, the Bolu tunnel, Anatolian Motorway, Turkey. Eng Geol 67(1–2):73–96

Gao M, Xie J, Gao Y et al (2021) Mechanical behavior of coal under different mining rates: a case study from laboratory experiments to field testing. Int J Min Sci Technol 31(5):825–841

Gao M, Hao H, Xue S et al (2022) Discing behavior and mechanism of cores extracted from Songke-2 well at depths below 4,500 m. Int J Rock Mech Min Sci 149:104976

He L, An XM, Zhao XB, Zhao ZY (2013) Investigation on strength and stability of jointed rock mass using three-dimensional numerical manifold method. Int J Numer Anal Meth Geomech 37(14):2348–2366

Hoek E, Diederichs MS (2006) Empirical estimation of rock mass modulus. Int J Rock Mech Min Sci 43(2):203–215

Hoek E, Marinos P (2000) Predicting tunnel squeezing problems in weak heterogeneous rock masses. Tunn Tunn Int 32(11):45–51

Jinpeng Z, Limin L, Chuanxiao L et al (2022) Mechanism and application of new prestressed yield bolt for controlling deep high-stress rock mass. Tunn Undergr Space Technol 119:104254

JTG 3370.1-2018 (2018) Specifications for design of highway tunnels. Ministry of Transport of the People's Republic of China, Beijing (**in Chinese**)

Kaya A, Karaman K, Bulut F (2017) Geotechnical investigations and remediation design for failure of tunnel portal section: a case study in northern Turkey. J Mt Sci 14(006):1140–1160

Kimura F, Okabayashi N, Kawamoto T (1987) Tunnelling through squeezing rock in two large fault zones of the Enasan Tunnel II. Rock Mech Rock Eng 20(3):151–166

Lai J, Wang X, Qiu J et al (2018) Extreme deformation characteristics and countermeasures for a tunnel in difficult grounds in

southern Shaanxi, China. Environ Earth Sci. https://doi.org/10.1007/s12665-018-7888-2
Li P, Zhao Y, Zhou X (2016) Displacement characteristics of high-speed railway tunnel construction in loess ground by using multi-step excavation method. Tunn Undergr Space Technol 2016(51):41–55
Li G, Hu Y, Tian S (2021) Analysis of deformation control mechanism of prestressed anchor on jointed soft rock in large cross-section tunnel. Bull Eng Geol Environ 80(12):9089–9103
Liu W, Chen J, Luo Y et al (2021) Deformation behaviors and mechanical mechanisms of double primary linings for large-span tunnels in squeezing rock: a case study. Rock Mech Rock Eng 54(5):1–20
Meguid MA, Rowe RK (2006) Stability of D-shaped tunnels in a Mohr-Coulomb material under anisotropic stress conditions. Can Geotech J 43(3):273–281
Meng L, Li T, Yun J et al (2013) Characteristics and mechanisms of large deformation in the Zhegu mountain tunnel on the Sichuan-Tibet highway. Tunn Undergr Space Technol Inc Trenchless Technol Res 37(Aug.):157–164
Merlini D, Stocker D, Falanesca M et al (2018) The ceneri base tunnel: construction experience with the southern portion of the flat railway line crossing the Swiss Alps. Engineering 4(002):235–248
Ng C, Lee K, Tang D (2004) Three-dimensional numerical investigations of new Austrian tunnelling method (NATM) twin tunnel interactions. Can Geotech J 41(3):523–539
Nguyen T, Ghabraie K, Thanh T (2015) Simultaneous pattern and size optimisation of rock bolts for underground excavations. Comput Geotech 66:264–277
Q/CR 9218-2015 (2015) Technical specification for monitoring measurement of railway tunnel. The Professional Standards Compilation Group of People's Republic of China, Beijing (**in Chinese**)
Rahimi B, Shahriar K, Sharifzadeh M (2014) Evaluation of rock mass engineering geological properties using statistical analysis and selecting proper tunnel design approach in Qazvin-Rasht railway tunnel. Tunn Undergr Space Technol Inc Trenchless Technol Res 41(Mar.):206–222
Sengani F, Zvarivadza T (2018) The performance of mechanical anchors in South African mechanized deep level gold mining, rock dynamics and applications 3. In: Proceedings of the 3rd international conference on rock dynamics and applications (RocDyn-3), vol 2018, p 681–687
Sun X, Li G, Zhao C et al (2019) Investigation of deep mine shaft stability in alternating hard and soft rock strata using three-dimensional numerical modeling. Processes 7(1):2
Sun XM, Chen F, He MC et al (2017) Physical modeling of floor heave for the deep-buried roadway excavated in ten-degree inclined strata using infrared thermal imaging technology. Tunn Undergr Space Technol 63:228–243
Sun X, Zhao C, Tao Z et al (2021) Failure mechanism and control technology of large deformation for Muzhailing Tunnel in stratified rock masses. Bull Eng Geol Environ 80(1):1–20
Tahmasebinia F, Zhang C, Canbulat I et al (2018) Numerical and analytical simulation of the structural behaviour of fully grouted cable bolts under impulsive loading. Int J Min Sci Technol 28(05):94–98
TB10003−2016 (2016) Code for design on tunnel of railway. Second Design Institute of China Railway, Beijing (**in Chinese**)
Tian H, Chen W, Tan X, Wang H, Tian T (2011) Study of reasonable support scheme for soft rock tunnel in high geostress zone. Chin J Rock Mech Eng 30(11):2285–2292
Wang H, Li H, Tang L et al (2022) Fracture of two threedimensional parallel internal cracks in brittle solid under ultrasonic fracturing. J Rock Mech Geotech Eng 14:757–769
Wu G, Chen W, Tian H et al (2018) Numerical evaluation of a yielding tunnel lining support system used in limiting large deformation in squeezing rock. Environ Earth Sci 77(12):439
Wu K, Shao Z, Qin S et al (2019) Mechanical analysis of tunnels supported by yieldable steel ribs in rheological rocks. Geomech Eng 19(1):61–70
Yang SQ, Miao C, Gang F et al (2018) Physical experiment and numerical modelling of tunnel excavation in slanted upper-soft and lower-hard strata. Tunn Undergr Space Technol 82:248–264
Zhang G, Wang F, Zhang H et al (2018) New stability calculation method for rock slopes subject to flexural toppling failure. Int J Rock Mech Min Sci 106:319–328
Zhang J, Zhou P (2017) Time-dependent jamming mechanism for single-shield TBM tunneling in squeezing rock. Tunn Undergr Space Technol 69(Oct):209–222
Zhu B, Ghee E (2011) Application of DEM in design of big tunnels in rocks at relatively shallow depth. In: Geomechanics and geotechnics: from micro to macro, vol 1 and 2, pp. 695–704
Zhu C, He MC, Jiang B et al (2021) Numerical investigation on the fatigue failure characteristics of water-bearing sandstone under cyclic loading. J Mt Sci 18(12):3348–3365